USING C. ELEGANS AS MODEL ORGANISM TO STUDY THE MODE OF ACTION OF A NATURAL TOXIN, PSYMBERIN

APPROVED BY SUPERVISORY COMMITTEE

Michael Roth, Ph.D.

Leon Avery, Ph.D.

Jef De Brabander, Ph.D.

Xiaodong Wang, Ph.D.

DEDICATION

I am grateful to people who made this journey possible. First, I would like to thank my mentor, Dr. Michael G. Roth for his patience, knowledge, and enthusiasm for science to guide me through the research. He is one of best mentor I even met. I would like to thank my dissertation committee members, Dr. Leon Avery, Dr. Jef De Brabander, and Dr. Xiaodong Wang, for their expertise to provide valuable advice and assistance that make this research more complete.

There are individuals who assisted me along the course of this study. The lab manager, Iryna Zubovych taught me all the techniques to do worm genetics. Eduardo Cardenas assisted with the forward genetic screen and microinjections. David Pedrón-Pérez and Matthew Evans revised my writings. Dr. Xin Jiang and Yu Feng provided the compounds used in the study. Dr. Noelle Williams ran samples on LC-MS for me. Without their effort, I could not finish this study.

Moreover, I thank God for giving me a lovely family to support my study in USA. My parents' continuous encouragement fueled me along the way. Other family members' caring also warmed my heart. Thanks to Hsing-Chun for helping me complete the last stage of this journey with prayers and God's grace, and who made this journey all worthwhile.

USING C. ELEGANS AS MODEL ORGANISM TO STUDY THE MODE OF ACTION OF A NATURAL TOXIN, PSYMBERIN

by

CHENG-YANG WU

DISSERTATION

Presented to the Faculty of the Graduate School of Biomedical Sciences

The University of Texas Southwestern Medical Center

In Partial Fulfillment of the Requirements

For the Degree of

DOCTOR OF PHILOSOPHY

The University of Texas Southwestern Medical Center

Dallas, Texas

August, 2011

USING C. ELEGANS AS MODEL ORGANISM TO STUDY

THE MODE OF ACTION OF A NATURAL TOXIN, PSYMBERIN

Publication No. _____

Cheng-Yang Wu, Ph. D.

The University of Texas Southwestern Medical Center, 2011

Supervising Professor: Michael G. Roth, Ph. D.

Psymberin is an extremely potent cytotoxin isolated from the marine sponges *Psammocinia* and *Ircinia ramose*. Several cancer cell lines are sensitive to psymberin, including breast, melanoma and colon cancer cell lines. Psymberin is the only member of the pederin natural product family that contains a dihydroisocoumarin side chain. The cytotoxicities of psymberin in various human tumor cell lines are between sub-nanomolar to nanomolar IC_{50}. Like pederin, the

first member of this natural product family, psymberin and mycalamide A inhibit translation *in vivo* and *in vitro*. This inhibition by psymberin is 40 to 100 fold more potent than cycloheximide, which inhibits >90% translation at 100 micromolar *in vivo*. In a SAR study, both the cytotoxicity of psymberin and psymberin-induced translation inhibition were attenuated by substituting the psymberin side chain with the pederin side chain. However, the attenuation of cytotoxicity was relatively greater than of translation. The stereo configuration and both side chains of psymberin are required for both inhibition of translation and cytotoxicity. The result of the SAR study suggests that additional bioactivity is contained in psymberin. Psymberin is at best a poor substrate for small molecule pumps in the cell.

Two separate forward genetics screens in *C. elegans* isolated seven independent psymberin-resistant mutants. In each the mutation was a C361T point mutation in the *rpl-41* gene that changes Pro65 to Leu65 in the protein coding sequence. The psymberin-resistant mutant strain DA2312 is resistant to psymberin only. This mutation did not appear to cause weaker binding of psymberin to the ribosome, but must allow translation to continue with the toxin bound.

There are additional modes of actions of psymberin compared to mycalamide A. The endogenous protein level of LC3, an autophagy marker, is decreased faster

with psymberin treatment than mycalamide A. In HT-29 cells, psymberin is capable of synergizing TNFα-induced necrotic cell death more efficiently than mycalamide A. The results from SAR study and from study of the psymberin-specific mutation in *C. elegans* suggest that psymberin may induce fast cell death through multiple pathways, including translation inhibition, apoptosis and necrosis. The structural uniqueness of psymberin has functional consequences suggesting that the mode of action of psymberin on the ribosome is different from other members of the pederin family.

TABLE OF CONTENTS

Chapter One Introduction 1

1.1. Pederin Family and Psymberin 1

1.2. Ribotoxic Effect Induced by Translation Inhibitors 9

1.3. Structure-Activity Relationship Study in Drug Discovery 13

1.4. *C. elegans* As Model Organism For Studying The Mode of Action of Small Molecules 18

1.5. Hypothesis and Research Approaches 22

Chapter Two SAR Study of Psymberin and Analogs in Translation Inhibition and Cytotoxicity 24

2.1. The Design of The SAR Study For Psymberin 24

2.2. The Translation Inhibition in Cell-based And in vitro Assays 27

2.3. The Cytotoxicity Assay And The Hint of Extra Biological Activities 32

2.4. Discussion 39

Chapter Three Forward Genetic Screen in *C. elegans* to Discover Psymberin-Resistance Mutations 42

3.1. Forward Genetic Screen 42

3.2 Mutation Mapping and Confirmation of Microinjection 47

3.3 Mutation Sequencing and Resistance Specificity 54

3.4 Discussion 57

Chapter Four A Comprehensive Study of The Mode of Action of Psymberin 60

4.1 Binding affinity of Psymberin to DA2312 Ribosome Is Not Significantly Weaker Than Wild-type Ribosome 61

4.2 Psymberin Does Not Interrupt Ribosome Assembly 64

4.3 Effect of Psymberin in Cell Death Pathways Other Than Apoptosis 67

4.4 Discussion 72

Chapter Five Conclusion and Future Directions 78

Methods and Materials 84

References 94

LIST OF FIGURES

Chapter One Introduction

Figure 1.1: Structures of representative compounds of each sub-category in the pederin family 4

Figure 1.2: Mycalamide A interacts with the 23S rRNA and L44e in the large ribosomal subunit..... 6

Figure 1.3: Structures of selected natural dihydroisocoumarins having biological activities 9

Figure 1.4: The ribotoxic stress response in the cell 12

Figure 1.5: A schematic view of the interaction between vancomycin analogs and the binding substrate..... 16

Figure 1.6: The structures and the relative inhibitory activities of statins..... 17

Figure 1.7: The life cycle of *C. elegans* 20

Figure 1.8: The *C. elegans* cell lineage in different developmental stages .. 21

Chapter Two SAR Study of Psymberin and Analogs in Translation Inhibition and Cytotoxicity

Figure 2.1: The psymberin analogs synthesized for SAR study 26

Figure 2.2: Representative translation-inhibition curves from a cell-based assay 28

Figure 2.3: Representative translation-inhibition curves from an *in vitro* translation assay 31

Figure 2.4: Representative cytotoxicity curves from cell-based CellTiter-Glo® assay 34

Figure 2.5: The HeLa cell survival curves with treatment of compound 37

Figure 2.6: The morphological change of HeLa cells with compound treatments 38

Chapter Three Forward Genetic Screening in *C. elegans* to Discover The Psymberin-resistant Mutation

Figure 3.1: Cytotoxicity curves of compounds on MDR mutant HeLa cells 43

Figure 3.2: A psymberin toxicity curve for the wild-type N2 strain 45

Figure 3.3: Resistance to psymberin is increased in line 29 after backcross twice with wild-type N2 worms 46

Figure 3.4: Using a SNP site to determine the origin of DNA 49

Figure 3.5: The percent of origin of DNA fragments in different positions on chromosomes 50

Figure 3.6: The percent of homozygous N2 samples at two end of chromosome II 51

Figure 3.7: The linkage map of the psymberin-resistance mutation on chromosome II 52

Figure 3.8: The linkage map of the psymberin-resistant mutation in a narrowed region on chromosome II..... 54

Figure 3.9: The sequencing trace for DA2312..... 56

Figure 3.10: The psymberin-resistant mutation does not confer resistance to the related toxin, mycalamide A..... 57

Figure 3.11: The point mutation in *rpl-41* sequence and the change in the amino acid sequence..... 59

Figure 3.12: Sequence alignment of RPL41 homologues 59

Chapter Four A Comprehensive Study of The Mode of Action of Psymberin

Figure 4.1: The binding of psymberin to mutant worm ribosome is weaker than to wild-type..... 62

Figure 4.2: The structural integrity of psymberin affects the binding affinity to ribosomes 63

Figure 4.3: HeLa cell lysates were sedimented on sucrose gradients to separate ribosomal subunits..... 65

Figure 4.4: The profile of ribosome subunits in the cytosolic fraction of HeLa cells with and without psymberin treatment does not change.... 66

Figure 4.5: Psymberin does not induce autophagy..... 68

Figure 4.6: Psymberin promotes the TNFα-induced necrosis in HT-29 cells..... 71

Figure 4.7: The aligned structures of RPL36a and L44e at the mycalamide A binding site. 74

Figure 4.8: The binding conformation of psymberin and mycalamide A in eukaryotic ribosome may be different from that in archaeal ribosome 75

LIST OF TABLES

Table I: The pharmacokinetic properties of statins …… 15

Table II: EC_{50} values of different psymberin analogs from in vivo assay 29

Table III: EC_{50} values of psymberin analogs in protein synthesis inhibition from *in vitro* assay 32

Table IV: IC_{50} Values of different psymberin analogs from cell viability assay . 35

Table V: The SNP sites examined in the genetic mapping 89

Chapter One
Introduction

The major source of modern drugs are natural products (1). The utilization of natural products as drugs can be traced back to sixty thousand years ago (2). Therefore, it has been a continuous interest to scientists to study the mode of action of different natural products, in order to develop new therapy for protecting and promoting the quality of human life. Among the different categories of natural products, the marine natural products have drawn much of the attention of scientists in recent years, not only for their challenging total synthesis, but also for the increasing number of potential therapeutic applications (3, 4). The goal of this study is to discover the mode of action of a marine natural product, psymberin, which could be a potential chemotherapeutic drug. This study provides the detailed modes of actions of psymberin in eukaryotic cells through combining a structure-activity relationship study, forward genetics in *C. elegans*, and biochemical studies with the techniques of molecular biology,

1.1 Pederin Family and Psymberin

The pederin family is a group of natural products which consists of more than 35 members, isolated from a variety of sources, from beetles to marine sponges (5).

There are five subcategories in the pederin family, including pederins (6-8), mycalamides (9-12), onnamides (13-16), theopederins (17-19) and psymberin (20, 21) (Figure 1.1). Despite the variety in source organisms, recent studies suggest the compounds of pederin family are produced by bacterial symbionts of the genus *Pseudomonas* sp. (5, 22). These bacteria live inside the organisms and secrete pederin analogs as chemical defense for the hosts. There are two common features of these natural products. First, they have the same amidyl tetrahydropyran main structural skeleton, which is the basis of the classification of this natural product family. The unified core structure suggests that these compounds could share at least one common biological activity (23). Second, most of the family members are toxic and act as translation inhibitors. The compounds being studied show antitumor activity as well. The antitumor efficacy and the cytotoxicity differ from member to member, due to the difference in side chain structures. (5).

Pederin (**1**) is the first member of the family. It is isolated from *Paederus* beetles and is the active compound to trigger vesicatory action to cause dermatitis (6). Because of medical needs, people are interested in studying the mode of action of pederin. The mode of action of pederin is the inhibition of more than 90% of DNA synthesis and protein synthesis in human cell lines at 20nM and 3nM, respectively. But RNA synthesis is not perturbed by pederin (24). The effects of

inhibiting both DNA synthesis and translation stop mitosis in HeLa cell after treatment with pederin at 2nM for two hours, and the cell cycle is arrested with chromosome condensation and the nuclei break down after 24 hours of treatment (24, 25). The precise molecular target of pederin is unknown, however, it binds to the 60S large ribosomal subunit (26).

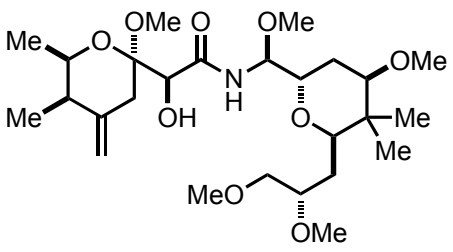

1

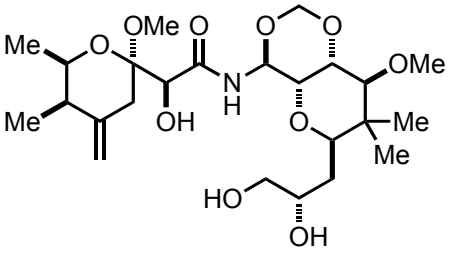

2

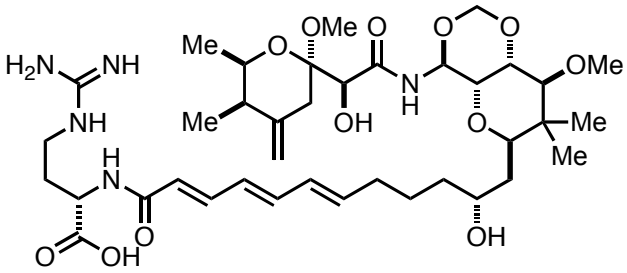

3

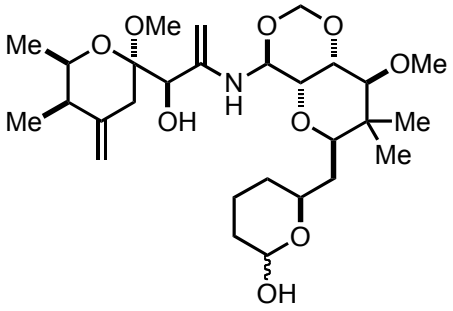

4

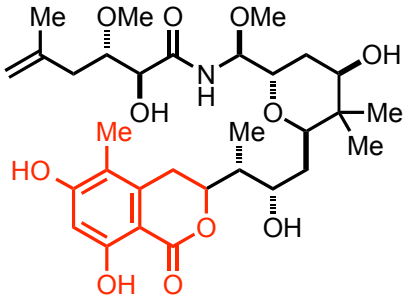

5

Figure 1.1 Structures of representative compounds of each sub-category in the pederin family. (**1**) Pederin, (**2**) Mycalamide A, (**3**) Onnamide A, (**4**) Theopederin A, (**5**) Psymberin. The structure in red is the dihydroisocoumarin side chain in psymberin, which is unique in the pederin family.

Mycalamide A (**2**) is another well-studied analog in the pederin family. It is isolated from the sponge of genus *Mycale* from New Zealand. Mycalamides were reported to have antiviral activity in the initial study (9). Like pederin's mode of action in HeLa cells, Mycalamide A inhibits both DNA synthesis and translation, but not RNA synthesis in the P388 lymphoma cell line. The efficacy and the cytotoxicity of mycalamide A are in the nanomolar range similar to pederin. Mycalamide A also demonstrates strong antitumor activity against various tumor models in mice, including leukemia, colon, melanoma and reticulum carcinoma (27). During the course of my research, in 2009, Moore and colleagues soaked the archaeal ribosome crystal in a solution containing mycalamide A to obtain the co-crystal structure of mycalamide A bound to a ribosome (28). In the crystal structure, mycalamide A sits in the interface of 23S ribosomal RNA (rRNA) and large ribosomal subunit protein L44e. The residues on C2394, C2395 and G2421 of the 23S rRNA are in close proximity to the oxygen atoms on the amidyl side chain. The residues on C2395 of 23S rRNA and the glutamine 44 of L44e are close to the tetrahydropyran ring. Both the residues on lysine 51 and lysine 54 of L44e are close to the diol side chain at the other side of the tetrahydropyran ring. These residues may form hydrogen bonds to stabilize the binding of mycalamide A to the large ribosomal subunit. The amidyl tetrahydropyran main skeleton occupies the same space as would the CCA terminus of a tRNA at the E-site in

the ribosome (Figure 1.2). Therefore, mycalamide A is categorized as an E-site inhibitor.

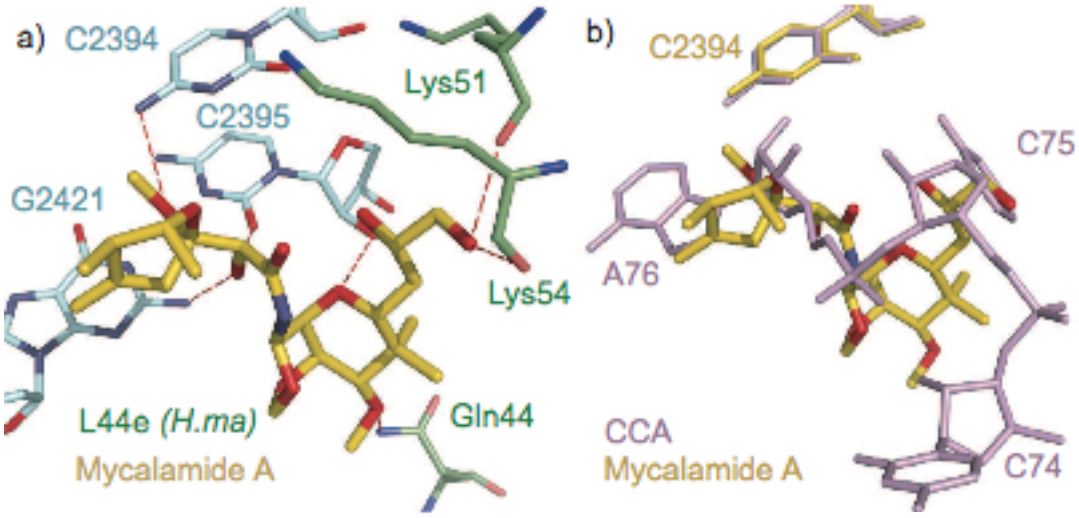

Figure 1.2 (Quoted from (28)) "Mycalamide A interacts with the 23S rRNA and L44e in the large ribosomeal subunit. (a) The complex mycalamide A forms with the *H.marismortui* ribosome is displayed. Mycalamide A is shown with C in gold, N in blue, O in red. 23S rRNA residues involved in hydrogen bonding are shown with C in light cyan, N in blue, O in red. L44e residues involved in drug interactions are shown with C in green, N in blue, O in red. Hydrogen bonds are shown as red dashes. E.coli base numbering is used for 23S rRNA residues and *H.marismortui* numbering is used for L44e protein. (b) Superposition of structures of mycalamide A bound to *H.marismortui* and the deacylated tRNA mimic CCA oligonucleotide bound to the same ribosome (PDB ID: 1QVG)(25). Mycalamide A is shown with C in gold; N in blue, O in red. CCA residues are shown in pink."

Psymberin (**5**) is the latest but most unusual member in the pederin family. It is isolated from the marine sponge *Psammocinia* sp. collected near Papua New

Guinea (20, 21). Like the rest of the compounds in the family, there is an amidyl tetrahydropyran structure as the main core skeleton. However, there are two unique structural features residing in psymberin. First, the terminus of the amidyl side chain on psymberin is a freely rotating isobutenyl group, unlike the more rigid pederic acid moiety in the other members of the pederin family. Secondly, the dihydroisocoumarin side chain on psymberin makes it the only compound with this type of side chain in the pederin family.

Dihydroisocoumarin is a core structure of various mycotoxins, the toxic secondary metabolites from fungi (Figure 1.3) (29-31). One of the most notorious natural dihydroisocoumarins is Ochratoxin A (OTA, **6**), which is one of the mycotoxins most often found in food contaminants (32). Ochratoxin A has a long half-life of 35 days in human serum. It induces kidney dysfunction when ingested by animals including humans (33). The biological activities of ochratoxin A are diverse. The major molecular target is phenylalanine-tRNA synthetase and as a consequence of lack of phenylalanine-tRNA, protein translation is inhibited. The side effects of ochratoxin A are the impairment of mitochondria membranes, elevated oxidative stress, and activation of c-jun amino terminal kinase (JNK) and extracellular regulated protein kinase 38 (p38)(34) The effect of activating the signaling cascade downstream of JNK and p38 is named ribotoxic stress, which will be described in the next section. At nanomolar concentration, ochratoxin A is

able to induce fast intracellular calcium oscillation in the immortalized human kidney epithelial cell-1 (IHKE-1). Under the same conditions, ochratoxin A promotes proliferation as well (35). There are other natural dihydroisocoumarins with different biological effects. Compound **7** is isolated from *Geotrichum* sp., one of the endophytic fungi. Compound **7** shows strong antimalarial toxicity to *Plasodium falciparum* K1, a multi-drug-resistant strain (29). Compound **8** is from a fungus named Nodulisporium sp.. It is a specific inhibitor of human DNA polymerase λ, at micromolar concentration (30). Compound **9** is a selective inhibitor of aromatase (CYP19), which is one of the cytochrome P450 enzymes. Compound **8** is from the plant *Xyris pterygoblephara*, and also demonstrates potent antifungal activity against dermatophyte fungi, which cause skin disease (36).

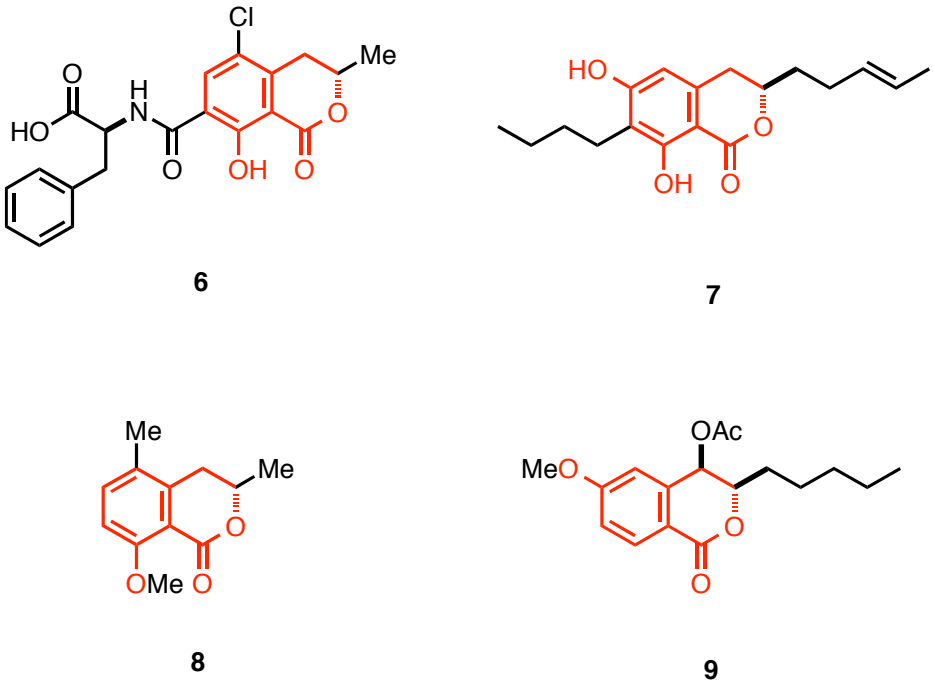

Figure 1.3 Structures of selected natural dihydroisocoumarins having biological activities. The structures in red are the dihydroisocoumarin cores in the natural products. (**6**) Ochratoxin A, (**7**) 3-(*R*)-7-butyl-6,8-dihy-droxy-3-pent-11-enylisochroman-1-one, (**8**) 3,5-dimethyl-8-methoxy-3,4-dihydroisocoumarin, (**9**) (3R,4R)-(-)-6-methoxy-1-oxo-3-pentyl-3,4-dihydro-1H-isochromen-4-yl acetate.

1.2 Ribotoxic Stress Induced by Translation Inhibitors

Ribotoxic stress is defined as the stress induced by damaging the ribosomal RNA. There are three types of stimuli which are able to trigger ribotoxic stress. The first type is the ribosome inactivating proteins (RIP), ricin A and α-sarcin. Both proteins catalyze sequence-specific damage to the a-sarcin/ricinA loop in 28S rRNA in rat liver cells, thus stopping the normal function of 28S rRNA in

translation. The second class of ribotoxic agents is translation inhibitors that act on rRNA, such as anisomycin. In 1997, Iordanov et. al. did a thorough study to show that not all of the translation inhibitors are capable of inducing ribotoxic stress. Only the translation inhibitors like anisomycin that interact with rRNA at a specific region can induce this response (37). Interestingly, two pederin family members, onnamide A and theopederin B activate JNK and induce apoptosis in mammalian cells (38). The third inducer of ribotoxic stress is UVB and UVC ultraviolet radiation. Light of both wavelengths activates the same stress-responsive signaling cascade as the other two types of stimuli (39, 40). The major effecter of ribotoxic stress in cells is the activation of c-jun amino terminal kinases (JNKs), also known as stress activated protein kinases. In mammalian cells, JNKs are one family of the mitogen-activated protein kinases (MAPKs), which serves as signaling mediators in the stress responsive signaling cascades. The upstream kinases of JNKs are MAPK kinases (MAPKKs) MKK4 and MKK7. Both MKK4 and MKK7 are activated by phosphorylation of upstream MAPKK kinases in response to exposure to stress (41). Activation of JNKs causes the transcription activators, such as c-Jun, ATF-2, and Elk1, to initiate the transcription of genes related to cell proliferation/survival and histone modification (42). The other direct targets of JNKs are insulin receptor substrate 1 (IRS-1) which is indispensable in metabolic and mitogenic pathways (43), and Bcl-2, which is an apoptosis regulator protein(44).

Interestingly, activation of JNKs is correlated with the induction of apoptosis in a cell type-dependent manner. Anisomycin is a potent translation inhibitor that induces strong ribotoxic stress. It triggers strong apoptosis in the human lymphoid cell line, HL-60 (45), but has a much weaker effect in HeLa cells (38). Activation of JNKs also sensitizes human cancer cells to death receptor-dependent apoptosis. In multiple glioblastoma cell lines, the addition of anisomycin with either the death receptor ligand anti-Fas antibody CH-11 or tumor necrosis factor-related apoptosis-inducing ligand (TRAIL) synergizes to induce apoptotic cell death. The combination of anisomycin and CH-11 up-regulates the level of the proapoptotic protein Bim but there is no change in the expression of the molecular brakes for apoptosis, such as Fas, FasL, FLIP and Fas-associated death domain (FADD) (46). Anisomycin also sensitizes PC3 prostate cancer cells to TRAIL-induced apoptosis. The phenotype can be rescued by overexpression of Bcl-2 (47). Further more, JNKs' activation triggered by anisomycin in HeLa cells elevates the reactive-oxygen species (ROS) level produced by mitochondria. The amplification of ROS level is also JNK-dependant because JNK knock-down decreases ROS production (48).

The outcome of exposure to ribotoxic stress in cells is obvious. It leads to cell death. But there are still missing links in the signaling pathway (Figure 1.4). The results above suggest that the stress comes from damaging the 28S rRNA in the

active ribosomes, followed by signaling of the stress-activated protein kinases to increase ROS production and induce apoptosis. At the same time, ribotoxins are also translation inhibitors, which also trigger apoptosis due to abolished protein synthesis. Therefore, the effect of ribotoxic stress is the combination of multiple reactions induced by ribotoxins.

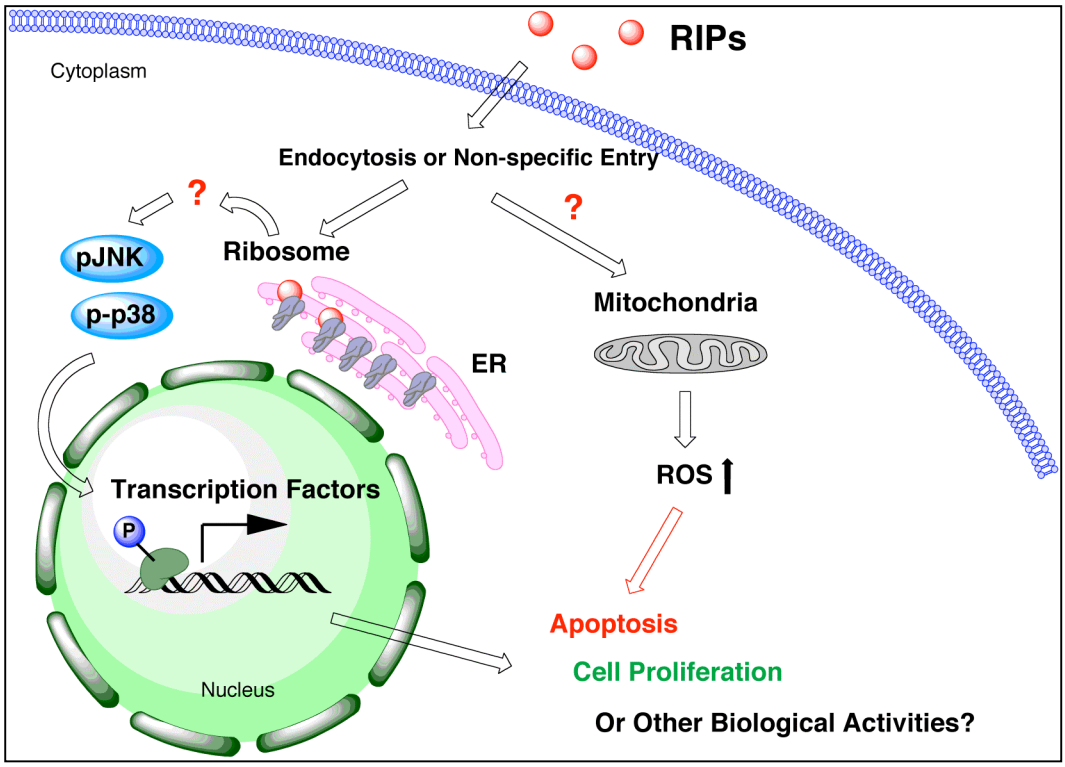

Figure 1.4 The ribotoxic stress response in the cell. (Modified from (42))

1.3 Structure-Activity Relationship Study in Drug Discovery

Structure-activity relationship (SAR) study is a powerful tool to determine the structural basis of bioactivity in a compound of interest. It is an integrative approach to combine organic synthesis and biological methods for characterization and manipulation of a compound. SAR study is important for drug discovery to select proper lead for further research (49-52). Taking vancomycin (**10**) as an example, it is a natural glycopeptide antibiotic used as the drug of last resort against Gram-positive bacterial infection. Concerned about growing numbers of vancomycin-resistant bacterial strains, people started to use SAR studies to reinforce the antimicrobial activity of vancomycin. The mode of action of vancomycin is to bind the L-Lys-D-Ala-D-Ala at C terminus of the peptidolglycan precursor, which is a building block of the bacterial cell wall. The cage-like structure of vancomycin blocks the polymerization of peptidolglycan to form the cell wall. There are five hydrogen bonds between vancomycin and the tripeptide sequence (Figure 1.5) (53). The vancomycin-resistant bacteria changed the last amino acid from D-Ala to D-Lactate. The loss of one hydrogen bond and the additional lone pair repulsion between two molecules resulted in a 1000 fold decrease in affinity. To eliminate the repulsive interaction, Crowley et al. modified the carbonyl group at residue 4 to a methylene group in vancomycin aglycon **11** and restored the antimicrobial activity in vancomycin-resistant VanA

bacteria (54). Modification on the N-terminus of vancomycin increased the affinity to the binding sequence by introducing more hydrogen bonds to the binding interaction. The modified vancomycin aglycon **12** also showed a boosted toxicity to VanA bacteria (55).

A SAR study reveals modifications not only to boost one specific bioactivity, but also to change multiple functional properties, such as seen in statins. Statins, or HMG-CoA reductase inhibitors, are a class of compounds capable of reducing the cholesterol level in blood by inhibiting the activity of HMG-CoA reductase. High cholesterol levels correlate to cardiovascular diseases and diabetes, which are among the top causes of death in the world. Therefore, several major pharmaceutical companies developed different statins (Figure 1.6) (56). There are two types of statins defined by the structure of the active core. The type 1 statins are the compounds with the hydroxyl lactone moiety, which will be hydrolyzed to hydroxyl acid under physiological conditions. They are derived or synthesized from natural sources (57). Type 2 statins are fully synthetic compounds with a hydroxyl acid moiety identical to that of HMG-CoA, a substrate of HMG-CoA reductase. Since the hydroxyl lactone is pharmacologically equivalent to the hydroxyl acid, the difference in IC_{50} comes from the hydrophobic structure away from the pharmacophore. The hydrophobic structure in statins plays an important role to stabilize binding to the HMG-CoA reductase. To avoid intellectual

property issues, each statin has slight chemical modification in the hydrophobic structure, which leads to different activities. In the co-crystal structures of statins bound to HMG-CoA reductase, only atorvastatin (Lipitor) and rosuvastatin (Crestor) have additional hydrogen bonds. Thus the IC_{50} values of these two statins are much lower than the other statins (56). In addition, the slight chemical modification in structure also changed the pharmacokinetic properties. Rosuvastatin has better body absorption, longer half-life in blood and less non-specific binding to other proteins. Thus, it is a more effective statin than others (Table I) (58).

Table I. The pharmacokinetic properties of statins. (Modified from (58))

	Simvastatin	Lovastatin	Fluvastatin	Atorvastatin	Rosuvastatin
Bioavailability (%)	<5	<5	29	12	20
t_{max} (h)	1.4-3.0	2.0-2.9	0.5-1.0	1.0-2.0	3.0-5.0
Elimination urine/ fecal (%)	13/60	10/70	5/95	2/98	10/90
Protein binding (%)	>95	>95	>95	>95	88
Elimination $t_{1/2}$ (h)	3	3-4	1	11-14	20
CYP Drug Intx (S, substrate; I, inhibitor)	3A4 (S)	3A4 (S)	2C9 (I)	3A4 (S)	2C9, 2C19

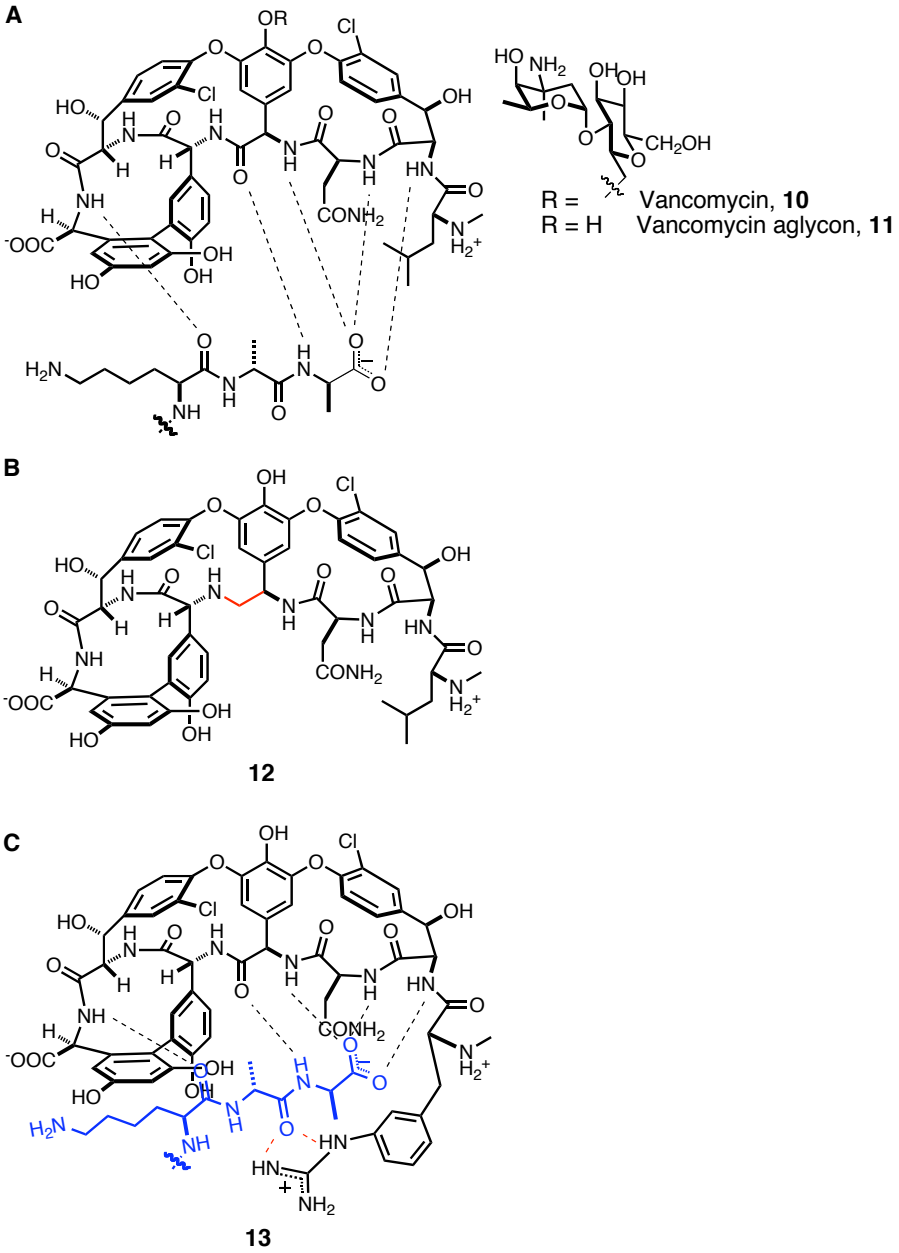

Figure 1.5 A schematic view of the interaction between vancomycin analogs and the binding substrate. A. The interaction of vancomycin (**10**) or vancomycin aglycon (**11**) with the L-Lys-D-Ala-D-Ala from bacteria. The dashed lines represent the hydrogen bonds. B. [Ψ[CH2NH]Tpg4]Vancomycin aglycon **12.** The modification on residue 4 (shown in red) reduces the repulsive interaction. C. The additional hydrogen bonds (in red) between the L-Lys-D-Ala-D-Ala (in blue) and modified vancomycin aglycon **13** (in black) (Modified from (53, 55))

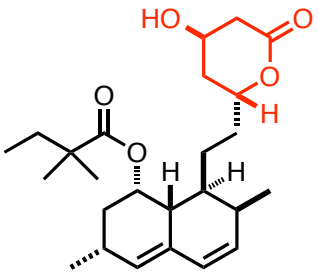

Simvastatin, **14**

IC_{50} = 11nM

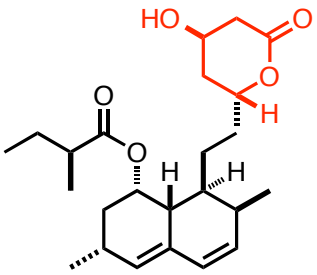

Lovastatin, **15**

IC_{50} = 150nM

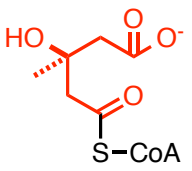

HMG-CoA, **16**

K_m = 4μM

Type 1

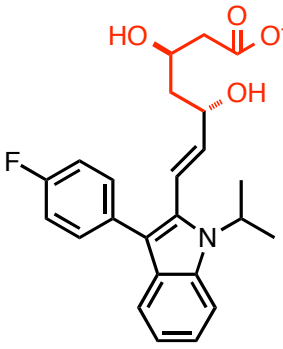

Fluvastatin, **17**

IC_{50} = 28nM

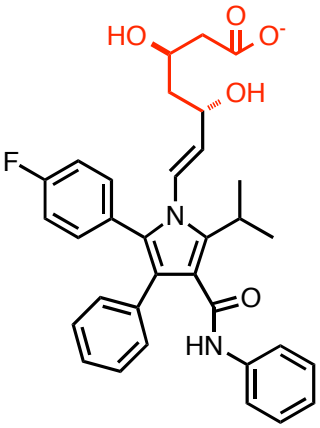

Atorvastatin, **18**

IC_{50} = 8nM

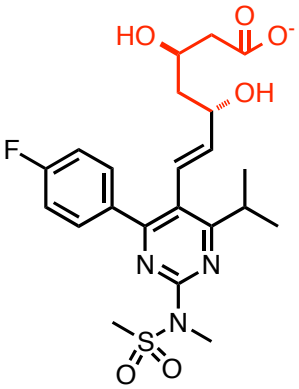

Rosuvastatin, **19**

IC_{50} = 5nM

Type 2

Figure 1.6 The structures and the relative inhibitory activities of statins. The structural features of two types of statins are illustrated. The IC_{50} values indicate the inhibition activities to the purified human HMG-CoA reductase. The HMG-like pharmacophore is shown in red. The hydrophobic skeleton is shown in black. (Modified from (56))

1.4 *C. elegans* As Model Organism For Studying The Mode of Action of Small Molecules

Model organisms are a powerful biological tool for drug discovery. With growing completions of genome sequencing in different species, forward genetic screening in model organisms is increasingly capable of unveiling the mode of action of small molecules. Furthermore, model organisms provide a full picture of the physiological impact from small molecules (59, 60). There are several well-developed model organisms from which to choose. The most well-known species are bacteria (60), yeast (61), *C. elegans* (62), *Drosophila* (63), zebrafish (64), and mice (65), each having various pros and cons. We choose *C. elegans* as the model organism to study the mode of action of psymberin, for the following reasons. First, *C. elegans* is easy to maintain with a short life cycle. *C. elegans* can be cultured on nematode growth medium (NGM) plates with *E coli* as the food source. Worms can also be cultured in a liquid medium, such as M9 buffer or S basal buffer with *E coli* suspension as the food source. For long-term storage, nematode strains can be frozen at minus 80 degree Celsius, just like cells. The life cycle of *C. elegans* is about 3 days from egg through the four stages of larva to mature adult (Figure 1.5), and the life span is approximately 2 weeks. The reproduction of the worms is robust. One adult worm can generate 300 eggs within its lifespan. Secondly, the genetics of *C. elegans* is well developed and the genome of *C. elegans* is fully sequenced (66). The large number of well-defined

single nucleotide polymorphism (SNP) sites and wide spectrum of visible markers facilitate mutation mapping. The common form of worms is the hermaphrodite, but males occur as 0.19% of the total population. The existence of the male allows genetic manipulation by mating males and hermaphrodites. There are also various deletion strains of *C. elegans* available for further characterization and confirmation of the results of screens for mutants. Thirdly, the worm is a simple but multicellular animal. The development of *C. elegans* is well documented. There are 959 somatic nuclei in the adult hermaphrodite. The lineage and the origin of each cell can be traced at each developmental stage (Figure 1.6). There are many visible phenotypes which can be used to score mutants (67, 68).

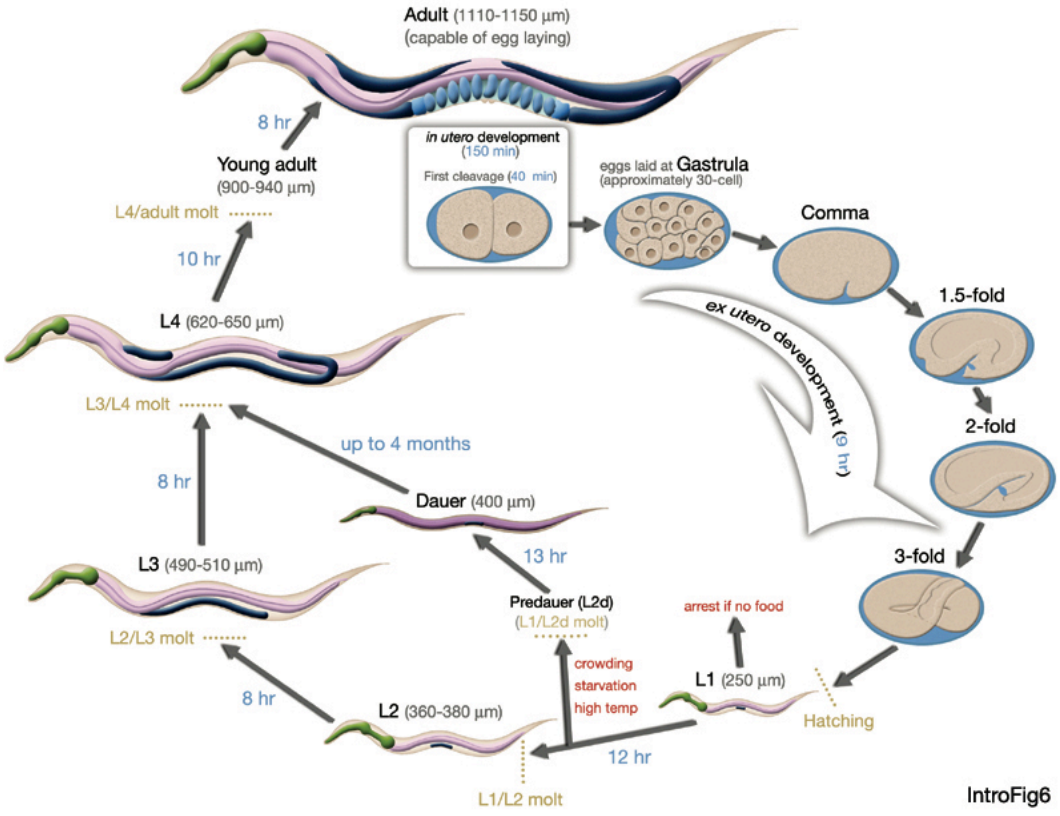

Figure 1.7 The life cycle of *C. elegans*. (Adapted from http://www.wormatlas.org/ver1/handbook/anatomyintro/anatomyintro.htm)

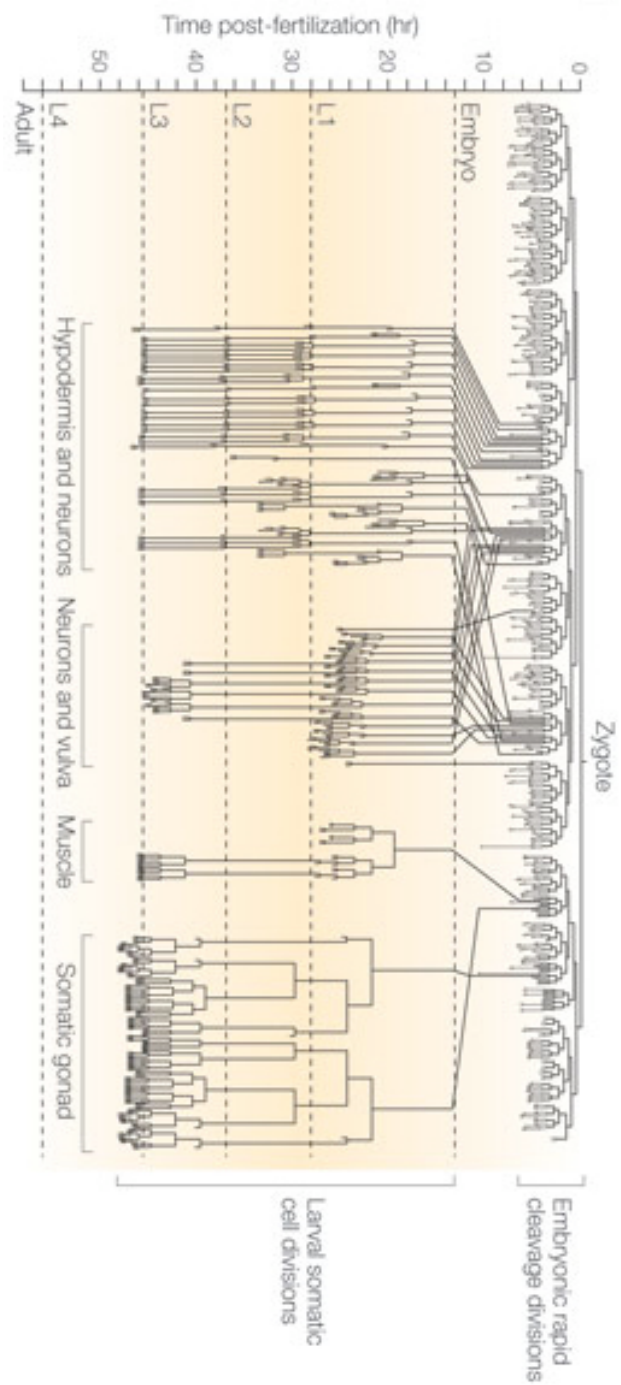

Figure 1.8 The *C elegans* cell lineage in different developmental stages. The vertical scale is the time post fertilization. Development stages from embryo to adult are divided by the dashed lines. (Adapted from (69))

The relevance of *C. elegans* to humans is reasonably high. According to genome sequencing and proteomics results, there are *C. elegans* homologs for 60-80% of human genes (70, 71). *C. elegans* is a good disease model for humans, as well. Based on the algorithm in the database OrthoDisease, out of 2,466 human disease genes, 533 orthologue clusters are identified in *C. elegans*, whereas there are 1,354 in mice (72). There are many biological processes that are conserved between human and *C. elegans*, such as the insulin/AKT pathway, oxidative stress, EGF/RAS pathways, neurodegeneration, innate immunity, the muscle system, etc (62). Despite the highly active efflux pumps in *C. elegans* which sets a potential limit for the study of small molecules, *C. elegans* is still a versatile model organism used to study the mode of action of small molecules.

1.5 Hypothesis and Research Approaches

Because of the unique dihydroisocoumarin side chain in psymberin, I hypothesized that psymberin might have biological effects other than simply inhibiting protein synthesis. To test this hypothesis, I performed a Structure-Activity relationship (SAR) study to dissect the active fragment of psymberin and a forward genetic screen in *C. elegans* to find the molecular target(s) of

psymberin. The effects other than translation inhibition were studied in human cells, as well.

Chapter Two

SAR Study of Psymberin and Analogs in Translation Inhibition and Cytotoxicity

2.1 The Design of The SAR Study For Psymberin

SAR study is a powerful tool to determine the structural basis of bioactivity in a compound of interest (49, 50, 52). To study the SAR of psymberin, eight psymberin analogs were synthesized in Dr. Jef De Brabander's laboratory (73). There are nine stereogenic centers in psymberin, of which the ones at positions C4 and C8 were altered from the *S* to the *R* configuration. 4-*epi*-psymberin (**20**) and 8-*epi*-psymberin (**21**) are the two epimers of psymberin with reversed stereogenic centers at C4 and C8, respectively. Analogs with different side chain truncations were also synthesized. The names and the structures are shown in Figure 2.1. Mycalamide A (**2**) was synthesized to serve as a representative compound of the rest of pederin family members. Psympederin (**22**) is a chimeric compound that has both the unique psymberin side chain at C1 to C8 and the characteristic pederin family side chain at C4 to C16. The 8-epimer of psympederin (**23**) was synthesized as a comparison for psympederin. Compound AS-2 (**24**) has eliminated the dihydroisocoumarin side chain of psymberin, whereas 175 (**25**) and 189-2 (**26**) have different truncations to remove the freely rotating double bond in

the amidyl side chain. The variety of the changes in these compounds provides a vast chemical space to begin the SAR study.

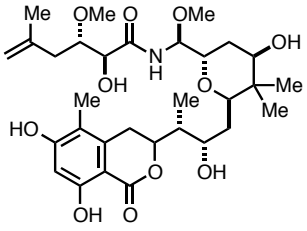

Psymberin, **5**

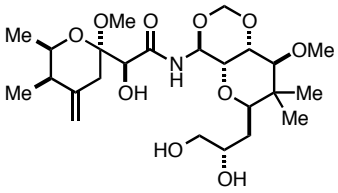

Mycalamide A, **2**

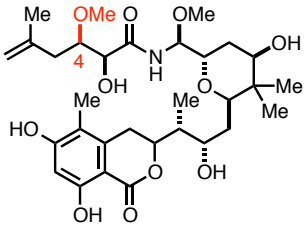

4-*epi*-Psymberin, **20**

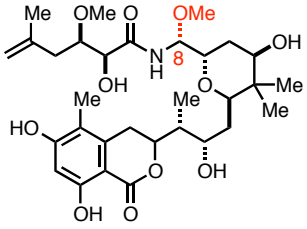

8-*epi*-Psymberin, **21**

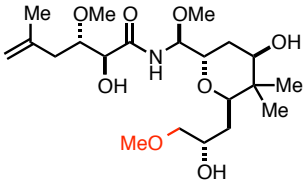

Psympederin, **22**

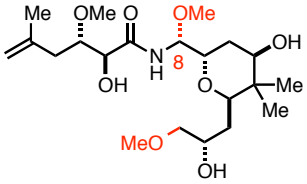

8-*epi*-Psympederin, **23**

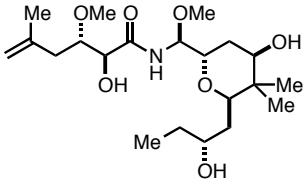

AS-2, **24**

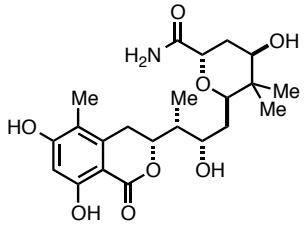

175, **25**

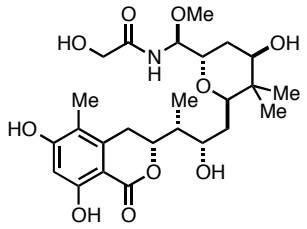

189-2, **26**

Figure 2.1 The psymberin analogs synthesized for SAR study. The chemical structure of every compound used in the SAR study is pictured. The functional groups in read show the modification at the specific site. The compounds **20**-**26** are the analogs with different truncations (shown in red).

2.2 The Translation Inhibition in Cell-based And *in vitro* Assays

To study the impact of structural changes on protein synthesis, two assays were used to measure the inhibition of translation induced by psymberin and the analogs. The first assay measured the total protein translation in HeLa or SK-MEL-5 cells through incorporation of radioactive ^{35}S-methionine into TCA-precipitable counts in the presence or absence of series of dilutions of the compounds (Figure 2.2). EC_{50} values could be obtained from these data by fitting it to a nonlinear regression for "log(inhibitors) vs. response—variable sloop" in Prizm. The result of such studies is shown in Table II. Psymberin potently inhibited translation with an EC_{50} value of 50nM in HeLa cells and 20nM in SK-MEL-5 cells. Cycloheximide, a commonly used translation inhibitor for mammalian cells, has an EC_{50} value of 4μM in HeLa cells and a similar value in SK-MEL-5 cells. Modifying the psymberin structure has a huge impact on inhibiting translation in the cell-based assay. The EC_{50} values of the two epimers, 4-*epi*-psymberin and 8-*epi*-psymberin, increased more than 20 fold compared to psymberin. The chimeric compound, psympederin, showed a similar fold change as well. Truncation of either side chain abolished the inhibition of translation dramatically. Compounds AS-2, 175 and 189-2 inhibited less than 20% of translation at 10μM, the highest concentration administrated from a 1mM stock solution. Thus, it is reasonable to predict that the EC_{50} values of AS-2, 175 and

189-2 are much larger than 100μM. Further more, alternating the stereogentic center at C8 in psympederin caused the same loss of translation as the truncated analogs. The results from the SK-MEL-5 cells are similar to those from HeLa cells.

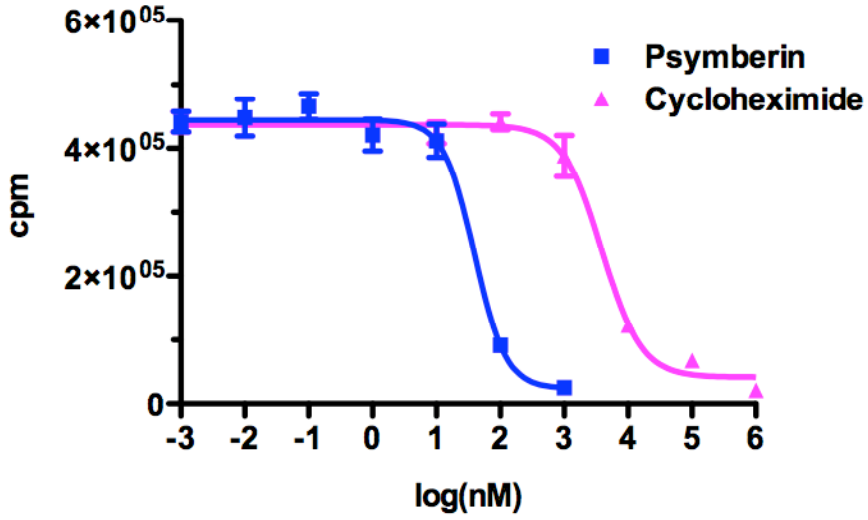

Figure 2.2 Representative translation-inhibition curves from a cell-based assay. Cells were treated with various doses of compounds, followed by labeling with ^{35}S methionine in the presence of the same doses of compounds. The x-axis presents the log values of the compound concentrations on a nanomolar scale. The y-axis is the radioactivity measured from the labeled protein in counts-per-minute (cpm). Data points are means with standard deviations. The blue square is psymberin, and the pink triangle is cycloheximide.

Table II. EC_{50} values of different psymberin analogs from in vivo assay†.

Compound	Hela* (μM)	SK-MEL-5** (μM)
Psymberin	0.05±0.03	0.02±0.01
Mycalamide A	0.04 0.09	0.09
Cyclohexmide	4±2	3 1.3
8-*epi*-psymberin	3.1 1.2	0.84
4-*epi*-psymberin	8.4 1.5	0.50
Psympederin	0.9 2.4	0.58
8-*epi*-psympederin	>100	>100
175	>100	N/A
AS-2	>100	N/A
189-2	>100	N/A

† Data shown in two numbers are results from two independent experiments. The other data are means±standard deviation from at least three independent experiments in triplicate. *R^2 values range from 0.931 to 0.994. **R^2 values range from 0.865 to 0.997.

The second assay is an *in vitro* translation assay in rabbit reticulocyte extract. The assay generates firefly luciferase from mRNA added to the extract and inhibition

of translation is determined as the decrease in activity of luciferase (Figure 2.3) as a function of concentration of the compound tested. EC_{50} values were obtained by fitting the data to an equation of "log(inhibitors) vs. response—variable sloop". All the analogs were tested in the *in vitro* translation assay. Similar to the cell-based assay, a trend of increasing EC_{50} values was observed (Table III). However, surprisingly, the fold change in EC_{50} values is much less than the values from the cell-based assay. The EC_{50} of psymberin in the *in vitro* assay is about four times larger (220nM) than the value from cell-based assay (50nM). But the EC_{50} values of the two epimers and of psympederin dropped to sub-micromolar concentration, which are no more than 4 fold of psymberin's. The EC_{50} of cycloheximide in the *in vitro* assay is close to the value from the cell-based assay. The truncated analogs showed the same decrease in translation-inhibition in the *in vitro* assay as in the cell-based assay. In general, the *in vitro* assay recapitulated the result from the cell-based assay to show the increased EC_{50} values of translation-inhibition with the alteration of psymberin structure.

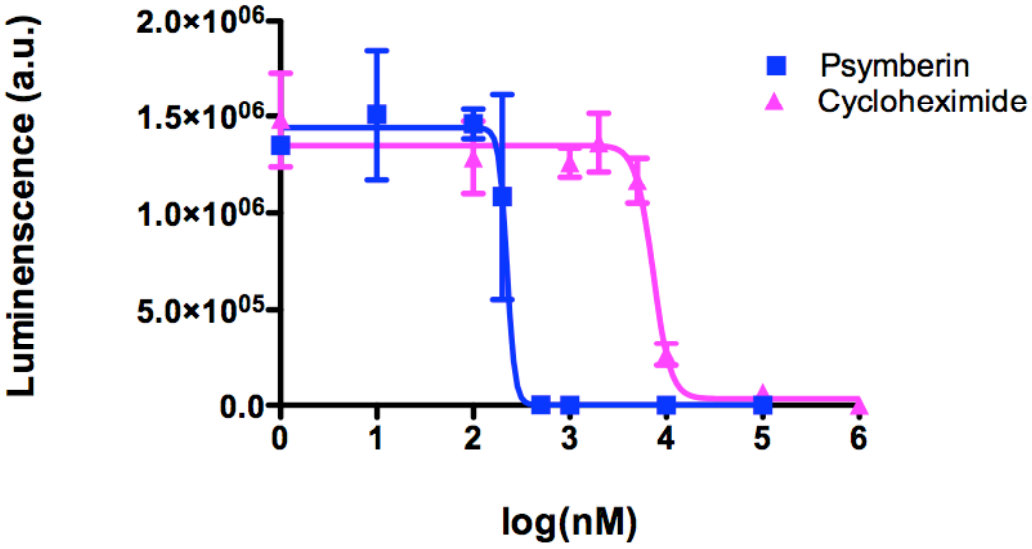

Figure 2.3 Representative translation-inhibition curves from an *in vitro* translation assay. The assay measures the activity of luciferase translated in the system. The cells were treated with various doses of compounds when the translation reaction was started. The x-axis presents the log values of the compound concentrations on a nanomolar scale. The y-axis is the intensity of luminescence in each treatment. Data points are means with standard deviations. The blue squares are psymberin, and the pink triangles are cycloheximide.

Table III. EC_{50} values of psymberin analogs in protein synthesis inhibition from *in vitro* assay.

Compound	EC_{50} (μM)*
Psymberin	0.22±0.04
Mycalamide A	0.12 0.21
Cyclohexamide	1.8 2.5
8-*epi*-psymberin	0.30±0.28
4-*epi*-psymberin	0.30 0.39
Psympederin	0.64±0.26
8-*epi*-psympederin	>100
175	>100
AS-2	>100
189-2	>100

*R^2 ranges from 0.90 to 0.995

2.3 The Cytotoxicity Assay And The Hint of Extra Biological Activities

To study the SAR of cytotoxicity, the CellTiter-Glo® luminescent assay, which measures cellular ATP concentrations, was used to measure cell viability with and without compound treatment (Figure 2.4). IC_{50} values were calculated by fitting the luminescence data to an equation representing a dose-response of inhibition of

luminescence in Prizm. The IC_{50} values of psymberin and the analogs are listed in Table IV. In HeLa cells, psymberin shows very potent cytotoxicity with the IC_{50} value of 0.6 nM. Similar to their effect on cell-based translation of inhibition, the cytotoxicity of the two epimer compounds was more than 150 fold less than psymberin. The truncated analogs could not even kill cells at concentrations below 10 μM. A similar trend is shown in SK-MEL-5 cells. However, psympederin showed a huge decrease in cytotoxicity compared to psymberin in both HeLa and SK-MEL-5 cell lines that was much larger than the difference in translation inhibition. The IC_{50} of cycloheximide was very close to the EC_{50} values from the translation inhibition assays. The mode of action of cycloheximide is to stop the translocation step of translation elongation by blocking the activity of the amino acid transferases (74). The similar IC_{50} and EC_{50} values of cycloheximide suggest that the cytotoxicity may originate from translation inhibition. The difference in psymberin between the EC_{50} and IC_{50} suggests that there might be an additional mechanism to increase cytotoxicity.

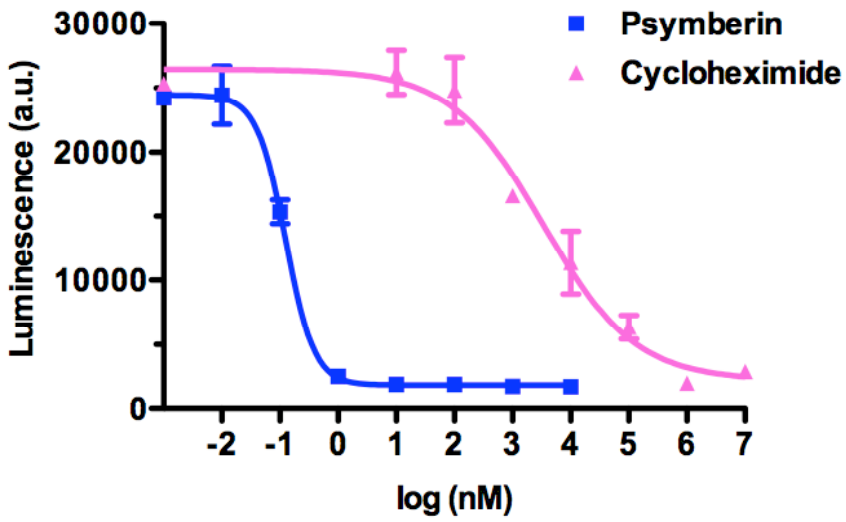

Figure 2.4 Representative cytotoxicity curves from the cell-based CellTiter-Glo® assay. The assay measures the ATP level in the cell. The cells were treated with various doses of compounds for 48 hrs before measuring the luminescence. The x-axis is the log of the compound concentrations in nanomolar unit. The y-axis is the intensity of luminescence in each treatment. The graph shows means with standard deviations of luminescence plotted against the concentration of each toxin. The blue squares are psymberin, and the pink triangles are cycloheximide.

Table IV. IC_{50} Values of different psymberin analogs from cell viability assay.

Compound	IC_{50} (nM)	
	HeLa	SK-MEL-5*
Psymberin	0.64±0.48	2.29±0.13
Mycalamide A	2.52±1.39	3.79±0.04
Cycloheximide	2242±1515	N/A
4-*epi*-psymberin	618.6±267.0	352.0±12.1
8-*epi*-psymberin	>1000	762.8±70.0
Psympederin	>1000	>1000
8-*epi*-psympederin	>1000	>1000
AS-2	>1000	N/A
175	>1000	N/A
189-2	>1000	N/A

*Data from (73)

Both psymberin and cycloheximide induce apoptosis in mammalian cells (75-77). The time to induce apoptosis in mammalian cells varies depending upon the inducer (78-80). In HeLa cells, the tumor necrosis factor-α (TNFα) induces apoptotic cell death by at least two hours after the caspase-8 activation (78). To probe the possibility that psymberin might induce cell death through mechanism in addition to inhibition of translation, I tested the survival of HeLa cells treated with psymberin at a concentration inhibiting 50% of translation. Cells were treated with psymberin for different periods of time in order to measure the

increase in toxic effects, while using cycloheximide as a control. Cells started to die after three hours of psymberin treatment. In the presence of the pan-caspase inhibitor Z-Vad-fmk, cell death was partially rescued within 8 hrs (Figure 2.5). However, there was no significant death of cells in treated with cycloheximide within 8 hrs. Psymberin induced cell death much more rapidly than cycloheximide. This result suggests that at 50% inhibition of protein translation, inhibiting translation and inducing apoptosis are not the only toxic effects from psymberin. To further characterize the effect of the fast cell death induced by psymberin, changes in the morphology of HeLa cells were investigated. Cells were treated for different period of time with compound at the level of more than 90% translation inhibition (Figure 2.6). HeLa cells started to round up after two hours in 1μM psymberin, and the population of rounded-up cells increased to more than 90% after six hours. In contrast, there was no significant change in the morphology of HeLa cells treated with 100μM cycloheximide treatment until 16 hrs. This result indicates that psymberin causes additional toxicity beyond inhibiting translation to induce such fast morphological change in cells.

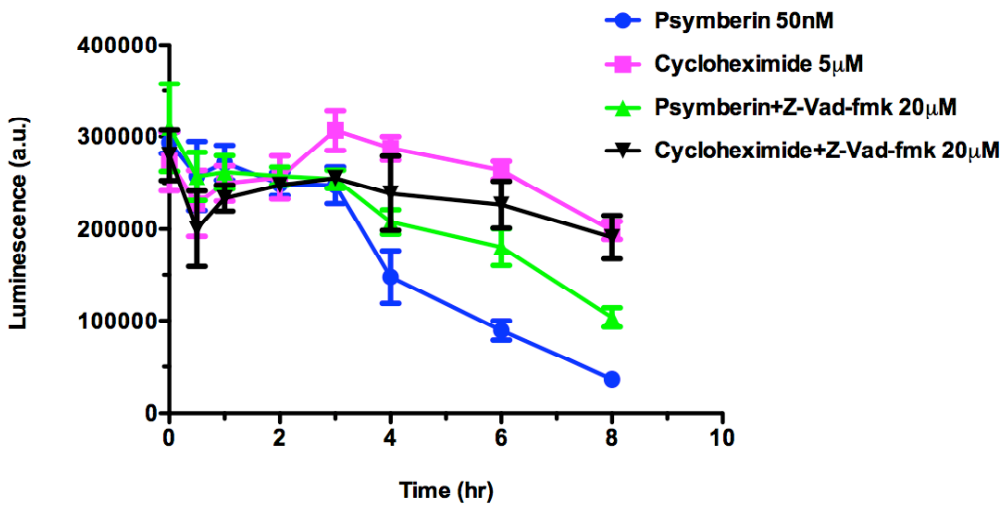

Figure 2.5 The HeLa cell survival curves with treatment of compound. The experiment was done using a cell-based CellTiter-Glo® assay. The assay measures cellular ATP levels. The cells were treated with compound in the presence of Z-Vad-fmk or not, for the times indicated on the x-axis. The y-axis is the intensity of luminescence measured in each sample. Means with standard deviations are plotted for each treatment condition. The blue solid circles represent data from psymberin, the pink squares data from cycloheximide, the green triangles from psymberin plus Z-Vad-fmk and the black flipped triangles from cycloheximide with Z-Vad-fmk.

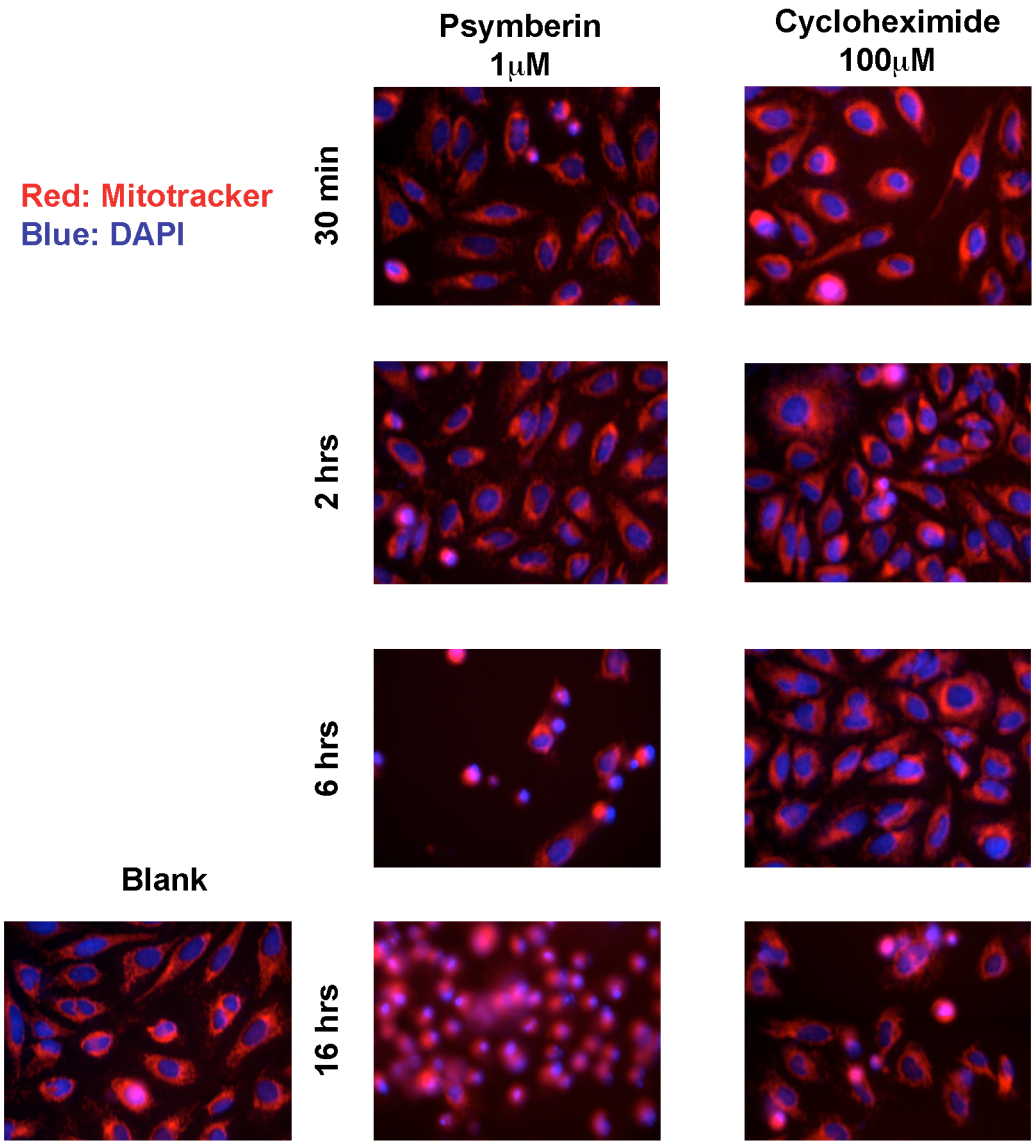

Figure 2.6 The morphological change of HeLa cells with compound treatments. The concentrations of psymberin or cycloheximide added were those that inhibit more than 90% of protein translation. The cells were treated with the dose and the time indicated in a 96-well plate. The images were taken at 20X magnification with 10X ocular. The focal plain is the same in each image.

2.4 Discussion

A precise chirality is important to the biological activity of many natural product-derived drugs. One well-known example is thalidomide. The *R*-form of thalidomide is a sedative, whereas the *S*-form is a teratogenic agent that disrupts limb development in animals, including humans (81). Surprisingly, the enantiomeric pure thalidomide is converted to racemic forms under physiological conditions (82). By affinity purification, the molecular target of toxic thalidomide was identified as cereblon, an E3 ubiqutin ligase (83). Given the fact that only the *S*-form is the active toxin, one may conclude that only the *S*-form thalidomide binds to cereblon and causes the destructive phenotype. The effect of changing chirality in psymberin may be different. Reduced activity on both inhibition of translation and cytotoxicity were observed for 4-*epi*-psymberin and 8-*epi*-psympederin (Table II to IV). In the literature, the (-)-psymberin, the mirrored form of psymberin, which has all nine stereogenic centers altered, showed a huge decrease in cytotoxicity, too (84). However, the fold change of reduced activity in the cell-based assay is different from the *in vitro* assay. In the cell-based assay for inhibiting translation, the fold change of the two epimers compared to psymberin is greater than 20 fold. In the *in vitro* translation assay, it is less than two fold. The fold change in IC_{50} (cytotoxicity) values of the two epimers is hundreds of times that of psymberin in CellTiter-Glow® assay. These huge contrasts suggest that a

single chirality change is not sufficient to cause significantly weaker binding to the ribosome, but it may be sufficient to affect the uptake or transportation of a compound by cells (85).

Structural integrity is important to psymberin, as well. When either side chain is truncated, both inhibition of translation and cytotoxicity decrease dramatically. Removing the terminal carbon-carbon double bound and the methoxy group at C4 on the amidyl side chain also abolished both translation inhibition and cytotoxicity (175 and 189-2, Table I to III). In the co-crystal structure of mycalamide A bound to the archaeal ribosome, there are eight possible hydrogen bonds between mycalamide A and the surrounding residues. It is surprising that even the removal of one hydrogen bonding site and a structure with no obvious interaction to it's neighborhood could cause such significant attenuation. On the other hand, the truncation of dihydroisocoumarin is fatal to the function(s) of psymberin (AS-2, Table I to III). Although compound AS-2 retains the full amidyl side chain on psymberin and the first hydroxyl group on the other side chain, it is not enough to avoid the loss of both biological activities. Interestingly, psympederin showed a greater loss in cytotoxicity than of translation inhibition. The structural feature of psympederin is the substitution of dihydroisocoumarin by the mono-methylated ethylene diol functionality that exists in pederin. Psympederin lost translation inhibition to a similar extent as the two epimers, but

showed a greater loss of cytotoxicity. These data suggest that dihydroisocoumarin is crucial for inhibiting translation. Further more, the dihydroisocoumarin substructure is very critical to induce cytotoxicity in psymberin.

The survival time course experiment and the observation of the changes in the morphology of HeLa cells suggest that there may be additional causes other than apoptosis for psymberin to induce cell death. Cycloheximide could not induce such fast cell death or morphology change within eight hours of treatment. The results from SAR study of both translation inhibition and cytotoxicity imply that the origin of the translation inhibition and the cytotoxicity is not only from the common amidyl tetrahydropyran core structure but also from the dihydroisocoumarin side chain. Our data also suggest that there is additional activity from psymberin to induce a fast cell death that makes psymberin different from cycloheximide. However, the SAR study did not reveal why psymberin alone of the pederin family has the biologically necessary dihydroisocoumarin side chain. Therefore, I used forward genetic screening in *C. elegans* to investigate this question.

Chapter Three

Forward Genetic Screen in *C. elegans* to Discover Psymberin-Resistance Mutations

3.1 Forward Genetic Screen

C. elegans eat bacteria for food and live in a relatively hazardous environment. There are many active efflux pumps expressed in worms to protect them from toxins produced by bacteria or other sources in the environment, (86, 87). Before I ran the forward genetic screen, it was important to test if psymberin was a good substrate of efflux pumps. In our lab, we generated a mutant HeLa cell line overexpressing multi-drug-resistant (MDR) pumps (88). The cytotoxicity of psymberin on these MDR mutant HeLa cells was tested and compared with the wild-type HeLa cells (Figure 3.1). Taxol, a known substrate of MDR pumps, was used as a positive control. The difference in the of IC_{50} of taxol in these two different cell strains is almost 1000 fold (Figure 3.1A), whereas the difference in IC_{50} of psymberin is about 10 fold (Figure 3.1B). Hemiasterlin is another small molecule toxin studied in our lab, which is a poor substrate for the MDR pump and has been used successfully to obtain drug-resistance mutants in *C. elegans*. The difference in IC_{50} for hemiasterlin in the two HeLa strains is about 10 fold as well. These results suggest that psymberin may not be a good substrate for MDR

pumps, which increases the probability of obtaining mutations in genes other than those encoding efflux pumps.

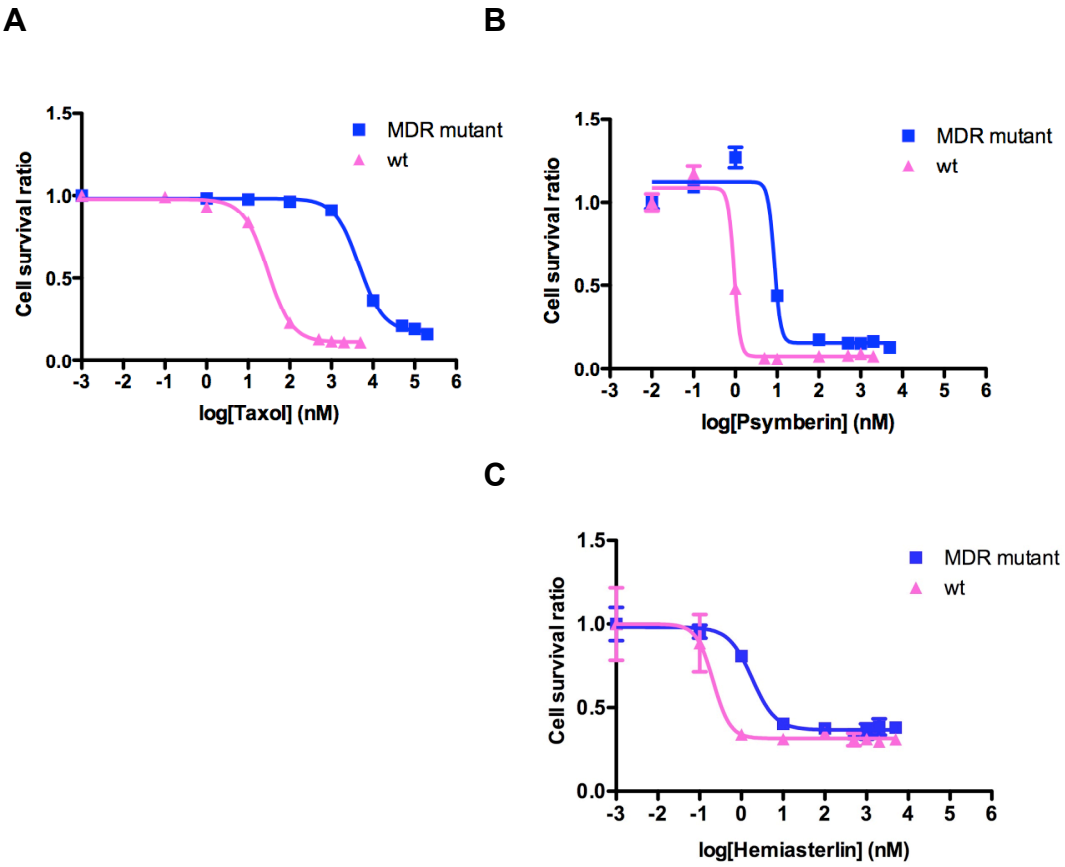

Figure 3.1 Cytotoxicity curves of compounds on MDR mutant HeLa cells. The cells were treated with various doses of compounds for 48 hrs before measuring the luminescence of CellTiter-Glo® reagent to determine ATP content of each sample, which is directly proportional to cell number. The graph shows means with standard deviations of luminescence plotted against the concentration of each toxin. The blue squares present data from MDR mutant HeLa cells, and the pink triangles are data from wild-type HeLa cells. The graph shows the result from A. Taxol treatment, B. Psymberin treatment, C. Hemiasterlin treatment.

C. elegans wild-type Bristol strain (N2) was used to perform the forward genetic screen. To set up the screen, I first determined the dose-response of worms to psymberin (Figure 3.2). The definition of drug resistance for this test is worms able to reproduce in the presence of the toxin. Therefore, only viable adult worms with eggs were scored. The same criterion was applied in the forward genetic screen for selecting psymberin-resistant mutants. Psymberin killed more than 95% of N2 worms above 2 μM concentration, and no L1 larva could grow or survive at 5 μM. Thus, 4.5 and 5 μM of psymberin were used in the forward genetic screen. About 50,000 N2 worms at the L4/young adult stage were treated with ethyl methanesulfonate (EMS) to generate random mutations. The eggs from F1 (first generation) progeny were treated with psymberin and the psymberin-resistant F2 (second generation) progeny were selected according to the criterion set earlier. The F2 survivors were tested again with 5 μM of psymberin in liquid culture to eliminate the false positive worms. There were only two worms left after the second round of screening. They were labeled 16 and 29, respectively. Line 29 was selected for further characterization. A backcross with wild-type N2 worms reduced background mutations. The effect of backcrossing was significant. After two times of backcrossing, the worms were healthier and the resistance to psymberin increased from 2 fold to 20 fold, compared to the wild-type N2 worms (Figure 3.3). To determine if the mutation in line 29 was dominant or recessive, male line 29 worms were mated with wild-type N2 hermaphrodites. All parental

worms produced psymberin-resistant F1 progeny, but 41 out of 74 F1 progeny produced psymberin-resistant F2 progeny. This result was consistent with a semi-dominant phenotype. The backcrossed line 29 was named as DA2312.

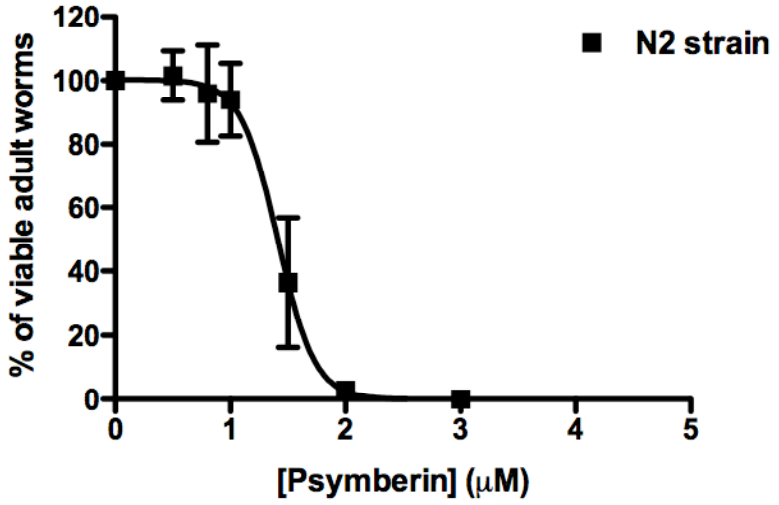

Figure 3.2 A psymberin toxicity curve for the wild-type N2 strain. Worms were cultured in M9 buffer with *E. Coli* HB101 as food. Serial concentrations of psymberin were added shown on the x-axis. The number of viable adult worms from L1 larva was scored. The means of survival expressed as a percentage of the mean of samples not treated with toxin were plotted on the y-axis with standard deviations.

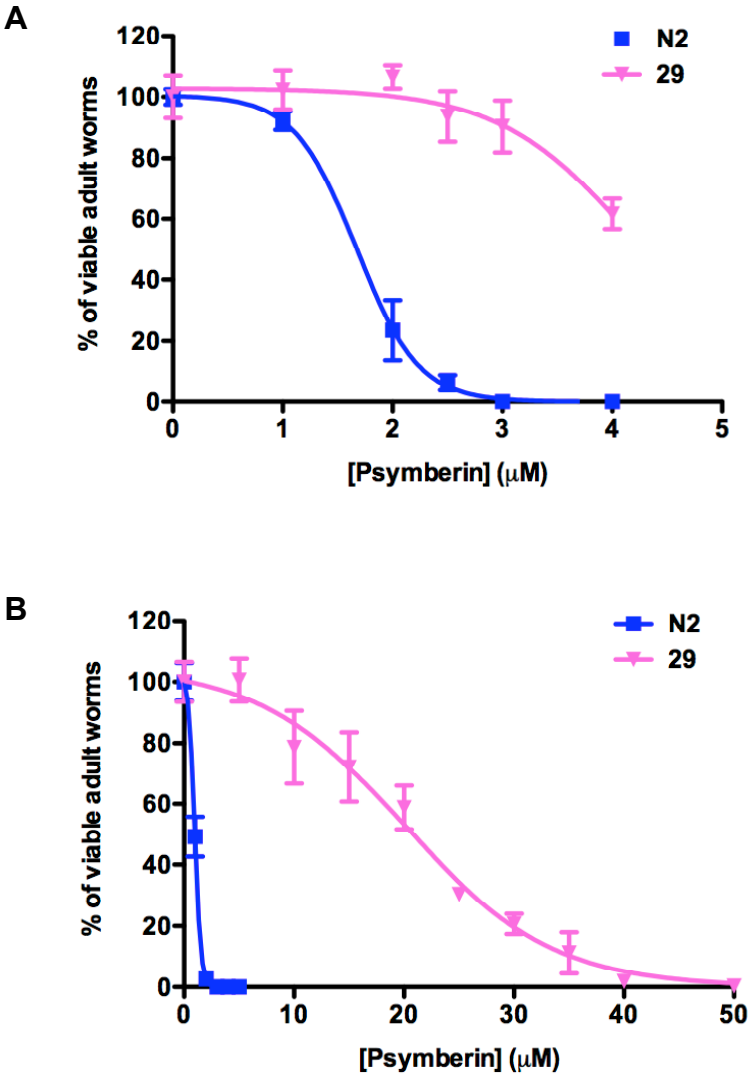

Figure 3.3 Resistance to psymberin is increased in line 29 after two backcrosses with wild-type N2 worms. Blue squares are the data from N2 samples. Pink triangles are the data from worm 29. The concentration of psymberin is indicated on the x-axis. A. The toxicity curve of psymberin to the two worm strains before backcrossing. B. The toxicity curve of psymberin to the two worm strains after backcrossing.

3.2 Mutation Mapping and Confirmation by Microinjection

Single nucleotide polymorphism (SNP) mapping is a technique used to map the site of mutations. The basis of SNP mapping is single nucleotide differences in DNA sequences of different worm strains, which distinguish the parental origin of a DNA fragment present in the progeny resulting from a mating between the two strains. The two strains used in my experiments were N2, the source of my mutant, and wild-type CB4856, hereafter referred to as CB. As an example of this technique, the SNP used in the center of chromosome II is at +0.11cM, position 22236 bp. In N2 worms, the nucleotide at the SNP site is an adenine (A), whereas it is a thymine (T) in the CB worms. The restriction enzyme DraI recognizes the TTTAAA sequence in N2 DNA, but not the TTTTAA in CB DNA. Therefore, when the DNA fragment containing this SNP is cloned, only the fragment of N2 origin is digested and cleaved by DraI. The result is visualized under UV by separating the DNA fragment on an agarose gel containing ethidium bromide (Figure 3.4).

Male DA2312 worms were mated with Hawaiian (CB) strain hermaphrodites, and 110 psymberin-resistant progeny were selected and grown on NGM plates individually. DNA from each progeny of the lines was subjected to the SNP mapping. First, the mutation-containing chromosome was identified. Because the

mutation is in a N2 background and is semi-dominant, every drug resistant worm should contain at least one copy of the N2 chromosome containing the mutation. All other chromosomes should be randomly distributed between N2 or CB origin in the progeny of the psymberin-resistant lines. The center of the chromosome is the place where the least recombination happens. The SNP sites close to the center of each chromosome were chosen to identify the mutant linkage. Chromosomes I and II showed lower ratios frequencies of homozygous CB SNPs compared to other chromosomes (Figure 3.5A). There are two genes on chromosome I involved in epistatic embryonic lethality in *C. elegans* (89). Therefore, the faction of homozygous CB in chromosome I is expected to be lower than the others even when the mutation is not linked to chromosome I (90). To further examine the mutation linkage to chromosome II, a DNA segment at +0.38cM on chromosome II was examined. The fraction of worms homozygous for the CB SNP at this position dropped to 1.8%. Thus, these data suggested that the mutation may link to chromosome II.

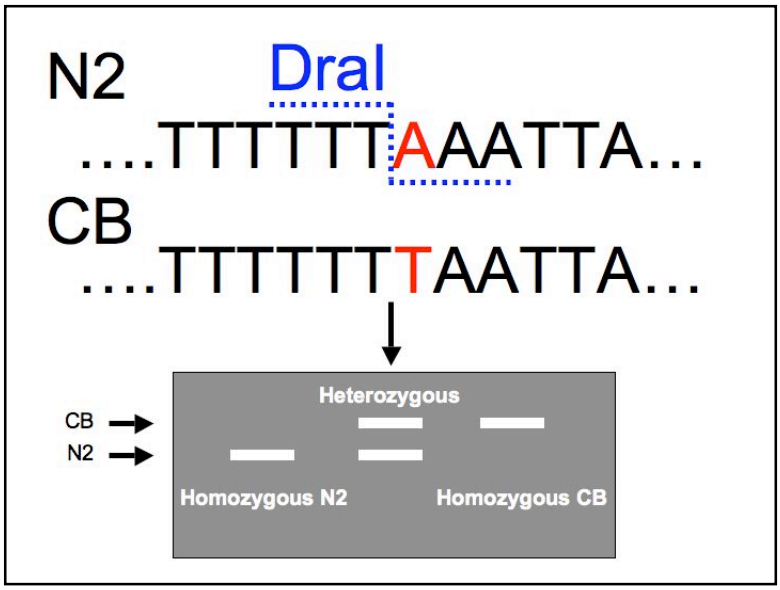

Figure 3.4 Using a SNP site to determine the origin of DNA. The SNP site is shown in red. The cleavage by DraI is shown in blue. The result of enzyme digestion is shown in the bottom of figure.

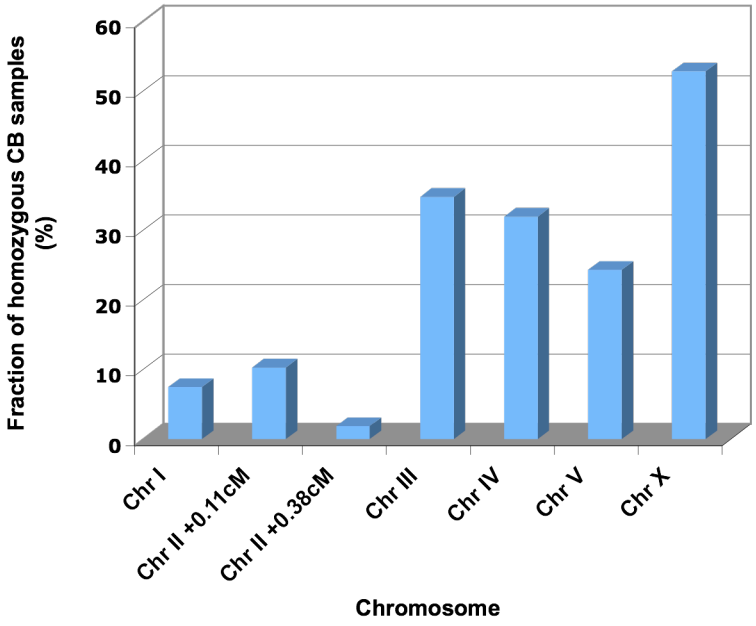

Figure 3.5 The percent of origin of DNA fragments in different positions on chromosomes. The fractions of worms homozygous for CB suggest the mutation is on chromosome I or II. The small fraction of homozygous CB samples on +0.38cM at chromosome II suggests the mutation is linked to chromosome II.

To narrow down the region containing the psymberin-resistant mutation, SNPs were used to determine which arm of chromosome II was linked to the mutation by calculating the fraction of drug-resistant worms homozygous for N2 DNA at the end of two arms (-15.9cM at the left arm and +15.77cM at the right arm). 37 samples with homozygous N2 at the center of chromosome II were examined in order to simplify the scoring and interpretation of the result. Since the recombination rate at end of chromosome is the highest, only the fraction of the

homozygous N2 was taken into account. The fraction of homozygous N2 was 62.2% at the +15.77cM, which is almost double of the fraction at -15.9cM (Figure 3.6). This result suggested that the mutation responsible for resistance to psymberin is linked to the right arm of chromosome II. SNP sites at five other positions on the right arm of chromosome II were examined to obtain a smaller region of chromosome II linked to resistance to psymberin (a linkage map). Based on the result from the linkage map, the region linked to psymberin-resistance is between to +1.38cM and +5.9cM.

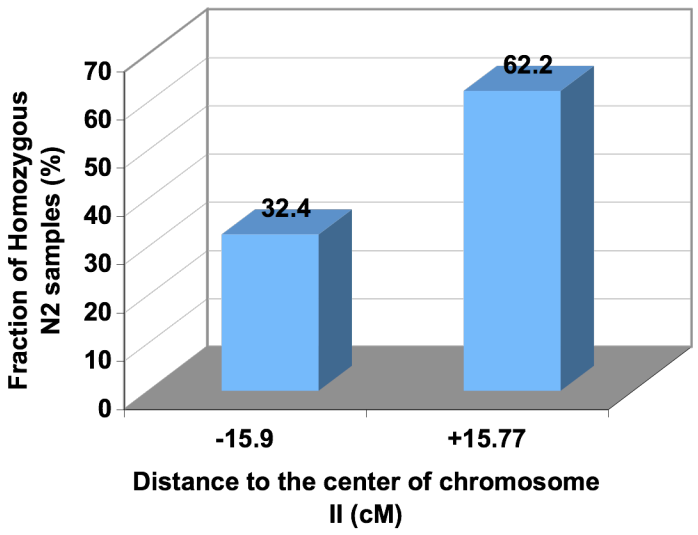

Figure 3.6 The percent of homozygous N2 samples at two end of chromosome II. Percentages were calculated by determining of strain of origin of the DNA fragments from 37 individual samples after crossing male DA2312 and CB hermaphrodites.

Position of SNP site (cM)	-15.9	+0.11	+1.38	+3.35	+5.9	+6.75	+8.15	+15.77
Sample								
5	H	N2	N2	N2		N2	N2	H
8	H	N2	N2	N2	N2	N2	H	CB
9	H	N2	N2	N2	N2	H	H	H
11	H	N2	N2	N2		N2	N2	CB
14	N2	N2	N2	N2		N2	N2	H
34	H	N2	N2	N2		N2	N2	H
41	N2	N2	N2	N2		N2	N2	H
42	H	N2	N2	N2		N2	N2	CB
44	N2	N2	N2	N2		N2	N2	H
45	H	N2	N2	H	H	H	H	H
46	N2	N2	N2	N2		N2	N2	CB
55	N2	N2	N2	N2		N2	N2	H
58	H	N2	N2	N2		N2	N2	H
61	H	N2	N2	N2		N2	N2	H
73		N2	N2	N2	N2	H	H	
82		N2	N2	N2	H	H	H	
91		N2	N2	N2	N2	N2	H	
99		N2	N2	N2	N2	CB	CB	
6	H	H	H	H	H	H	N2	N2
21	CB	H	N2	H		N2	N2	N2
28	CB	H	N2	N2		N2	N2	N2
33	CB	H	N2	H		N2	N2	N2
35	H	H	H	N2	N2	N2	N2	N2
51	H	CB	H	N2	H	H	H	N2
52	H	CB	H	N2	N2	N2	N2	N2
53	H	CB	H	N2	N2	N2	N2	N2
71	CB	H	H	H	H	N2	N2	N2
84	H	H	H	N2	H	H	N2	N2
86	H	H	H	N2	N2	N2	N2	N2

Figure 3.7 The linkage map of the psymberin-resistance mutation on chromosome II. N2 represents a homozygous N2 DNA at the locus, H in yellow blocks represents the heterozygous DNA, CB in orange blocks represents homozygous CB DNA at the indicated SNP site.

To further reduce the region, two visible markers, *dpy-10* (+0.00cM) and *rol-1* (+6.89cM) were chosen for a three-point mapping. Male DA2312 worms were mated with either *rol-1* or *dpy-10* hermaphrodites to generate double mutants.

Males of each double mutant were mated with Hawaiian hermaphrodites to obtain psymberin-resistant F2 progeny lacking the visible marker, indicating a worm having chromosome recombinations between the mutation site and the site of the visible marker mutation. Then the individual psymberin-resistant progeny were subjected to the SNP site examination between +1.38cM and +5.9cM to identify an interval on the chromosome containing the recombination site. This generated a new linkage map reducing the region linked to the mutation (Figure 3.8). The data shown in the Figure 3.8 suggested that the psymberin-resistant mutation was located in the region between +3.1cM and +3.5cM on chromosome II.

Position of SNP site (cM)	+1.38	+1.77	+3.1	+3.35	+3.5	+4.04	+4.11	+5.9	+6.75
Sample									
6	H	H	H	N2			N2		
62	H	H	H	N2			N2		
77	H	H	N2	N2			N2		
96	H	H	H	N2			N2		
105	H	H	H	N2			N2		
1				N2	N2	N2	CB		
2				N2	H	H	H	H	H
6				N2	H	H	CB		
7				N2	N2	CB	CB	CB	CB
16				N2	N2	N2	CB	CB	CB
29				N2	N2	N2	CB		

Figure 3.8 The linkage map of the psymberin-resistant mutation in a narrowed region on chromosome II. The upper group of samples were from the *dpy-10 ad2312sd* X CB cross and the bottom group was from the *rol-1 ad2312sd* X CB. N2 represents a homozygous N2 DNA, H in yellow blocks represents a heterozygous DNA, and CB in orange blocks represents a homozygous CB DNA at indicated SNP site.

3.3 Mutation Sequencing and Resistance Specificity

In the region between +3.1cM and +3.5cM, there are 221 genes. 86 genes are identified with known functions, 29 genes without known functions and 106 sequences are predicted as possible genes. Since psymberin is a translation inhibitor, three genes in this region were selected for sequencing: *rpl-41*, which encodes a 60S ribosomal large subunit protein, *rps-9*, which encodes a 40S

ribosomal small subunit protein and *R03D7.4*, which encodes a RNA binding protein with a human homologue, elongin. Only *rpl-41* showed a mutation, a C to T substitution at position 361 in the protein coding sequence (Figure 3.9). The other line, 16, also showed the same point mutation. Another independent forward genetic screen confirmed the result. The screen was started with about 1 million F1s after EMS-mutagenesis and resulted in the isolation of 5 non-sibling F2 progeny resistant to 5 μM of psymberin. All 5 worms contained the same-point mutation, a C to T transition in the *rpl-41* gene. This mutation would change a codon specifying proline to one coding leucine. Thus, from two independent mutagenesis experiments a total of seven independently-derived worms were obtained that were able to grow to gravid adult stage in 5 μM psymberin and all of them contained the identical mutation. This suggests that there is a very limited number of mutations, perhaps only one, capable of producing the phenotype selected in these two screens. To further confirm the phenotype, a complementation experiment was done by injecting mutant *rpl-41* DNA into wild-type N2 worms, in combination with unlinked *rol-6* DNA as a positive control. I isolated 17 stable transgenic roller worms, and 16 of 17 roller progeny produced psymberin-resistant progeny. Thus the mutation and the phenotype were confirmed.

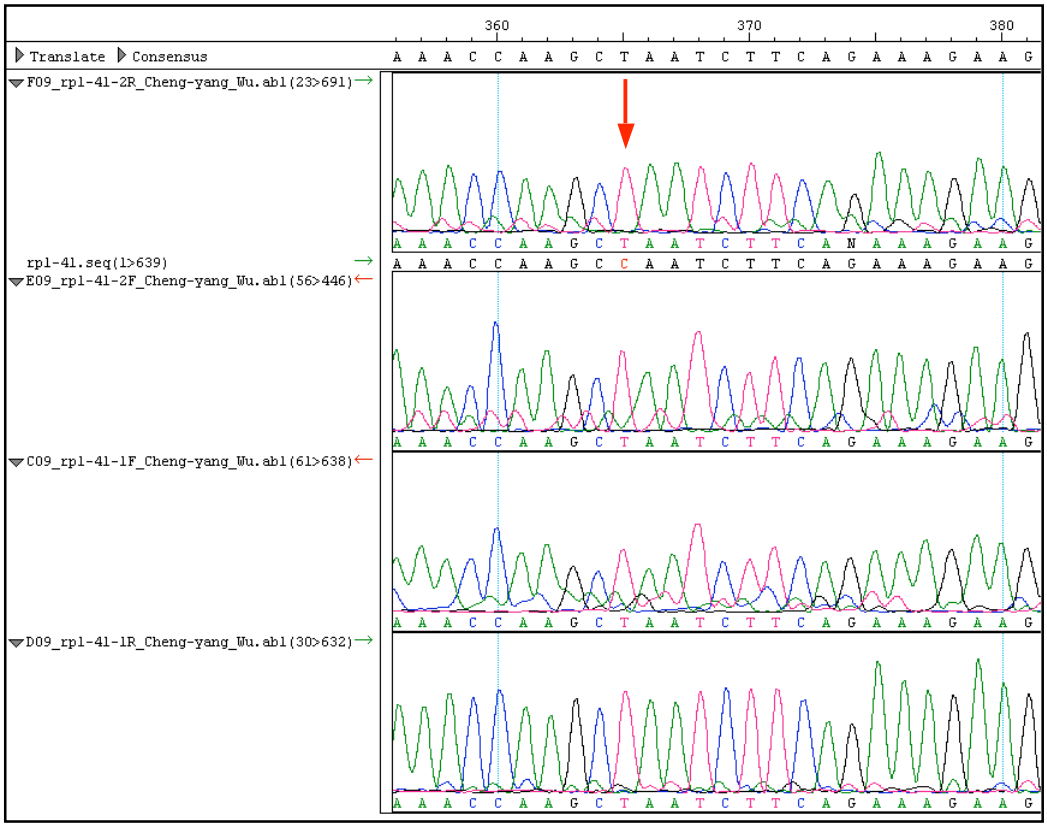

Figure 3.9 The sequencing trace for DA2312. The wild-type *rpl-41* sequence is shown in black next to the second green arrow from the top. Two sets of primers that covered the entire coding region of *rpl-41* are shown at the left column. The sequence and the nucleotide traces are shown in the right column. The mutation site is indicated by red arrow. Adenine is in green, thymine is in red, guanine is in black and cytosine is in blue. The position of nucleotide is indicated on the top.

Due to the structure similarity in the pederin family, one wonders if the mutation in *rpl-41* would also confer resistant to other pederin family toxins. Wild-type N2 and DA2312 worms were treated with various concentrations of mycalamide A to test for drug-resistance. Interestingly, DA2312 showed the same sensitivity as the

wild-type N2 worms (Figure 3.10). This result suggested that the mutation in *rpl-41* is psymberin-specific.

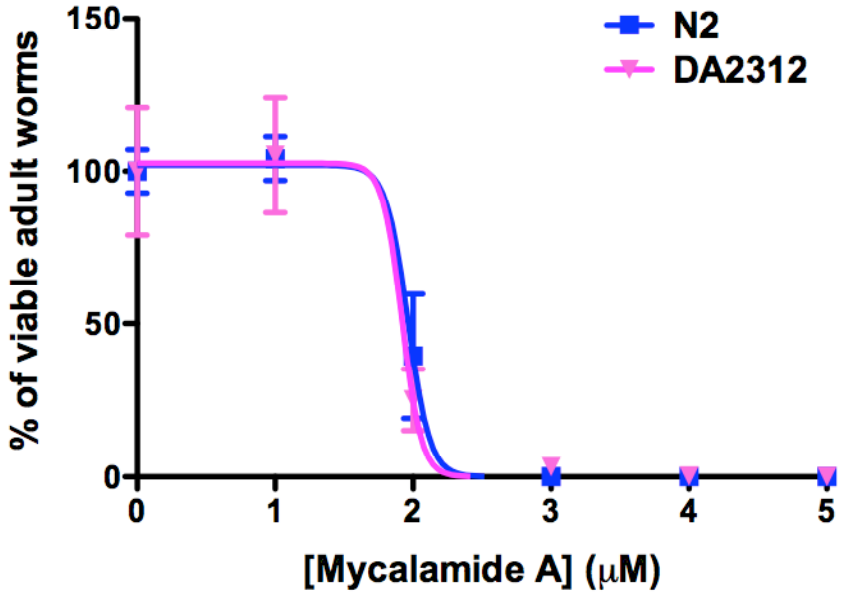

Figure 3.10 The psymberin-resistant mutation does not confer resistance to the related toxin, mycalamide A. The toxicity curves for mycalamide A on DA2312 and N2 worms are presented. Blue squares indicate data from N2 samples, pink triangles the data from DA2312.

3.4 Discussion

Seven psymberin-resistant mutants identified in two independent screens all had the identical point mutation in *rpl-41*. This suggests that the number of different possible mutations in *C. elegans* capable of producing resistance to psymberin is

small. The C to T point mutation is the type of transition caused by EMS (91) and causes a change of proline to leucine in the coding sequence, which is a significant structural change (Figure 3.11). The change from a rigid proline to a relatively flexible leucine may cause structural changes in the pocket where psymberin binds to the ribosome. However, if so, these changes do not affect the binding of a structurally similar toxin, mycalamide A, suggesting that the changes must be rather local. In addition, the sequence homology of RPL41 is highly conserved in eukaryotic organisms (Figure 3.12). It is likely the drug-resistant phenotype of this mutation would be conserved in higher eukaryotic organisms as well.

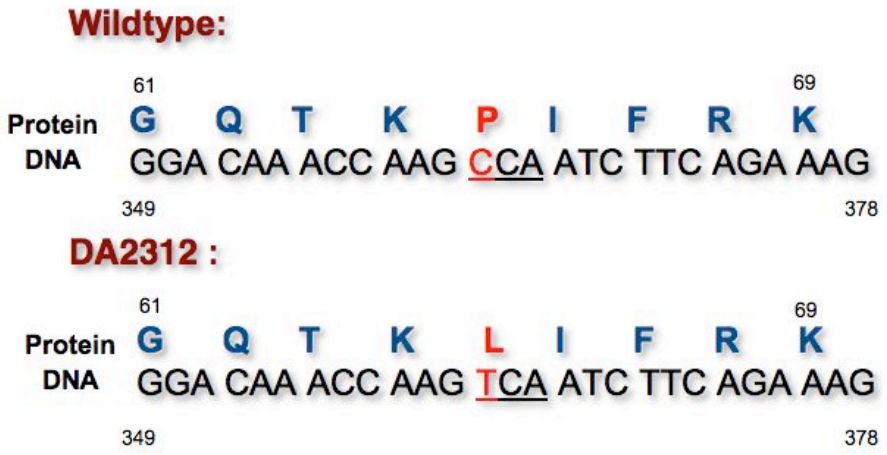

Figure 3.11 The point mutation in *rpl-41* sequence and the change in the amino acid sequence. The DNA sequence is in black and the protein sequence is in blue. The mutation is indicated in red. The positions of sequences are indicated.

```
Yeast RPL42ap        MVNVPKTRKTYCKGKTCRKHTQHKVTQYKAGKASLFAQGKRRYDRKQSGFGGQTKPVFHK
C. elegans RPL-41    MVNVPKARRTFCDGK-CRKHTNHKVTQYKKGKESKFAQGRRRYDRKQSGFGGQTKPIFRK
Drosophila RPL36a    MVNVPKQRRTFCK-K-CKVHKLHKVTQYKKSKERKGAQGRRRYDRKQQGFGGQTKPIFRK
Mouse RPL36a         MVNVPKTRRTFCK-K-CGKHQPHKVTQYKKGKDSLYAQGKRRYDRKQSGYGGQTKPIFRK
Human RPL36a         MVNVPKTRRTFCK-K-CGKHQPHKVTQYKKGKDSLYAQGKRRYDRKQSGYGGQTKPIFRK
Human RPL36al        MVNVPKTRRTFCK-K-CGKHQPHKVTQYKKGKDSLYAQGRRRYDRKQSGYGGQTKPIFRK

Yeast RPL42ap        KAKTTKKVVLRLECVK--CKTRAQLTLKRCKHFELGGEKKQKGQALQF
C. elegans RPL41     KAKTTKKIVLRMECTE--CKHKKQLPIKRCKHFELGGQKKSRGQVIQF
Drosophila RPL36a    KAKTTKKIVLRMECTE--CKYRKQTPLKRCKHFELGGDKKRKGQMIQF
Mouse RPL36a         KAKTTKKIVLRLECVEPNCRSKRMLAIKRCKHFELGGDKKRKGQVIQF
Human RPL36a         KAKTTKKIVLRLECVEPNCRSKRMLAIKRCKHFELGGDKKRKGQVIQF
Human RPL36al        KAKTTKKIVLRLECVEPNCRSKRMLAIKRCKHFELGGDKKRKGQVIQF
```

Figure 3.12 Sequence alignment of RPL41 homologues. RPL41 is a highly conserved protein. The residues in black are the conserved residues. The blue colored residues indicate less conserved positions. The proline in red is the mutation site.

Chapter Four

A Comprehensive Study of The Mode of Action of Psymberin

In previous chapters, a thorough SAR study was reported that examined the structural origin of biological activities in psymberin. A hint of possible additional activities was discovered by testing for cell survival 8 hrs after addition of psymberin. Psymberin killed cells faster than did cycloheximide when both were present at concentrations that inhibited translation to the same extent. On the other hand, the only psymberin-resistant mutation I found in seven independently derived worms demonstrated a significant 20-fold increase in resistance compared to wild-type worms. This mutation, which caused a proline to leucine mutation at residue 65 on RPL41, suggests that the ribosome is the target of psymberin. Therefore, to further characterize the possibility of additional activities of psymberin and the impact of the point mutation, several biochemical and cell-based methods were used to examine the impact of the mutation on the binding affinity of psymberin to ribosomes and on ribosome assembly. Also, the ability of psymberin to induce autophagy and necrosis was investigated.

4.1 The Binding Affinity of Psymberin to the DA2312 Ribosome Is Not Significantly Weaker Than to the Wild-type Ribosome

The mutation conferring resistance to psymberin might affect the affinity of binding of the toxin to the ribosome, or might affect some consequence of this binding. To investigate these possibilities, the binding affinity of psymberin was measured. Initially, we tried to use NMR to study the binding of psymberin to the worm ribosome. The advantages of using NMR are that NMR can probe weak interactions and measure any conformational change of psymberin occurring after binding (92). However, even though we observed a change in both signal intensity and chemical shift of the only aromatic proton in the dihydroisocoumarin side chain, this signal was insufficient to provide an accurate calculation of a binding constant. Therefore we used a different method, modified from the literature (26), to measure the binding affinity of psymberin to ribosomes. The free psymberin content in a reaction solution at equilibrium of binding to ribosomes was quantified by LC-MS and binding curves were plotted (Figure 4.1A). The calculated K_d of psymberin bound to a wild-type ribosome is about 50% less than that of mutant (Figure 4.1B), but by T-test did not reach a 95% confidence level of being significantly different. This result suggested that the change from proline to leucine may not significantly weaken the binding of psymberin to the mutant ribosomes, although it results in almost a 20-fold increase in resistance to the toxic effects of psymberin. Thus, this amino acid change must allow translation to

proceed with psymberin bound, possibly by making a portion of RPL41 more flexible..

A

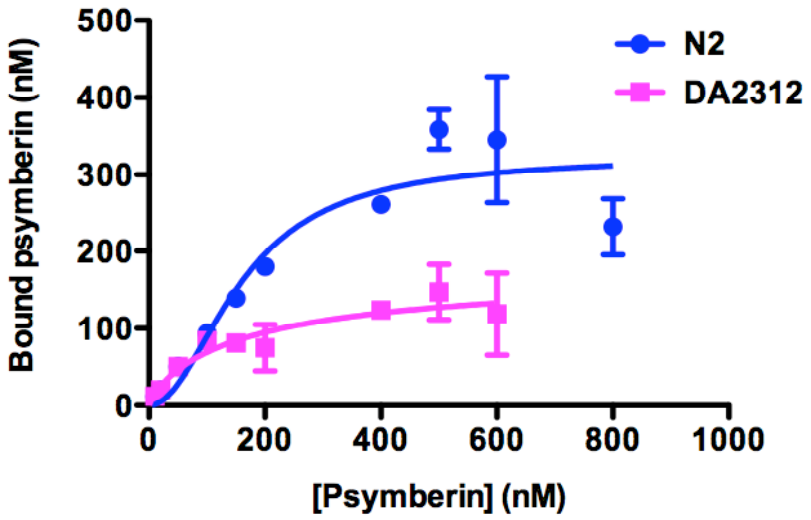

B

K_d (nM)	
N2	DA2312
97.6±20.7	146.9±18.4

Figure 4.1 The binding of psymberin to mutant worm ribosome is weaker than to wild-type. A. Concentrations of psymberin in bound state vs. total were plotted. The curves of wild-type (-■-) and DA2312 (-●-) are shown. B. The K_d values are presented as "mean ± SEM" from at least 3 experiments done in triplicate.

The effect of changing the structure of psymberin to the binding affinity for ribosomes was also studied. The amount of free compound AS-2 or 175 after

equilibrium binding between 200nM of compound and worm ribosomes was quantified (Figure 4.2). Under these conditions, there was no binding between AS-2 and worm ribosome. 175 had either very weak or no interaction with wild-type ribosome while showing no binding to DA2312 ribosomes. In contrast, under these conditions, psymberin bound to wild-type ribosomes strongly and more weakly to mutant ribosomes. These data correlate with the SAR study in mammalian cells that indicated that the dihydroisocoumarin is an important moiety for the biological activities of psymberin and suggest that loss of this side chain results in weak or no binding to ribosomes.

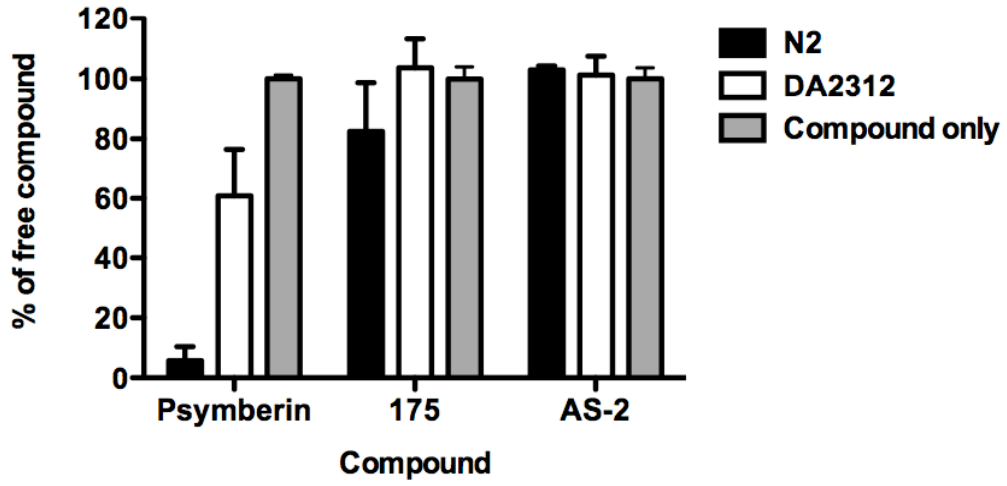

Figure 4.2 The structural integrity of psymberin affects the binding affinity to ribosomes. Psymberin and truncated analogs were tested for binding affinity to worm ribosomes. The percentages of free compound at the equilibrium of binding interaction to N2 (black) and DA2312 (white) ribosomes are plotted. The data is normalized to samples containing only compound and no ribosomes.

4.2 Psymberin Does Not Interrupt Ribosome Assembly

Inhibition of ribosomal subunit synthesis is a secondary effect of a group of antibiotics that inhibit bacterial protein synthesis with different modes of action on the ribosome. For an example, neomycin binds to the 23S rRNA in the 30S subunit at the helix H69. The binding of neomycin prevents ribosome recycling by stabilizing the 70S ribosome structure (93). In addition to the interaction described above, neomycin also inhibits the synthesis of the 30S subunit in *E. coli* (94). To test if psymberin stops protein synthesis with the additional activity of disrupting ribosome assembly, a ribosome assembly assay was performed. Both nuclear and cytosolic ribosome profiles were obtained from HeLa cell lysates isolated from cells that had been treated with 1μM psymberin for 6 hours. The ribosome profile in the nucleus had no change in pattern but the total amount of two subunits was lower in the psymberin-treated cell (Figure 4.3). No change in ribosome profile was found in the cytosol (Figure 4.4). To test if psymberin interrupts the assembly of RPL36a/al to ribosome, the protein content of RPL36a in each fraction was measured and shown to correlate with the 60S subunit and 80S/polysome peaks in the cytosolic ribosome profile (Figure 4.4). These data suggested that psymberin does not interrupt the ribosome assembly or the incorporation of RPL36a into the ribosome. However the amount of the two

subunits in the nucleus was affected, probably as a consequence of inhibition of protein translation.

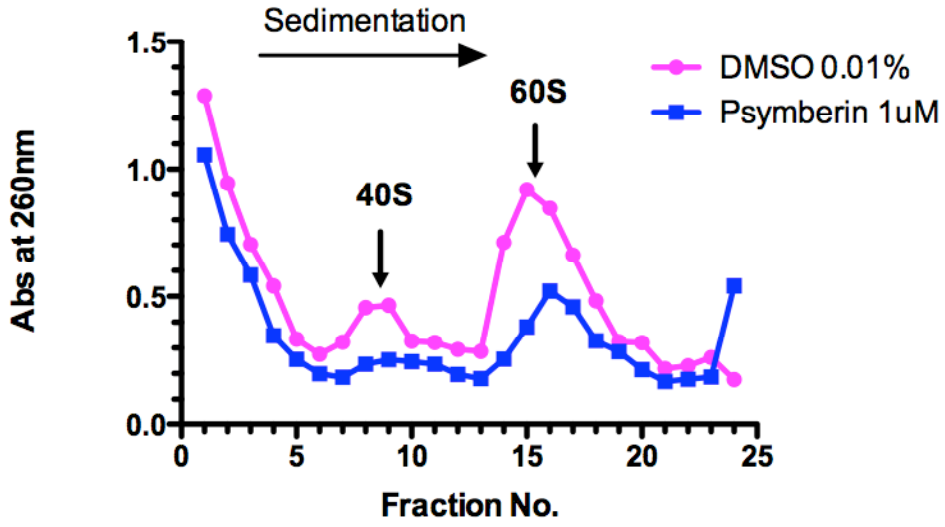

Figure 4.3 HeLa cell lysates were sedimented on sucrose gradients to separate ribosomal subunits. The profiles of ribosomal RNA in the nuclear fraction from HeLa cells treated with psymberin (-■-) or with the DMSO carrier (-●-) are shown.

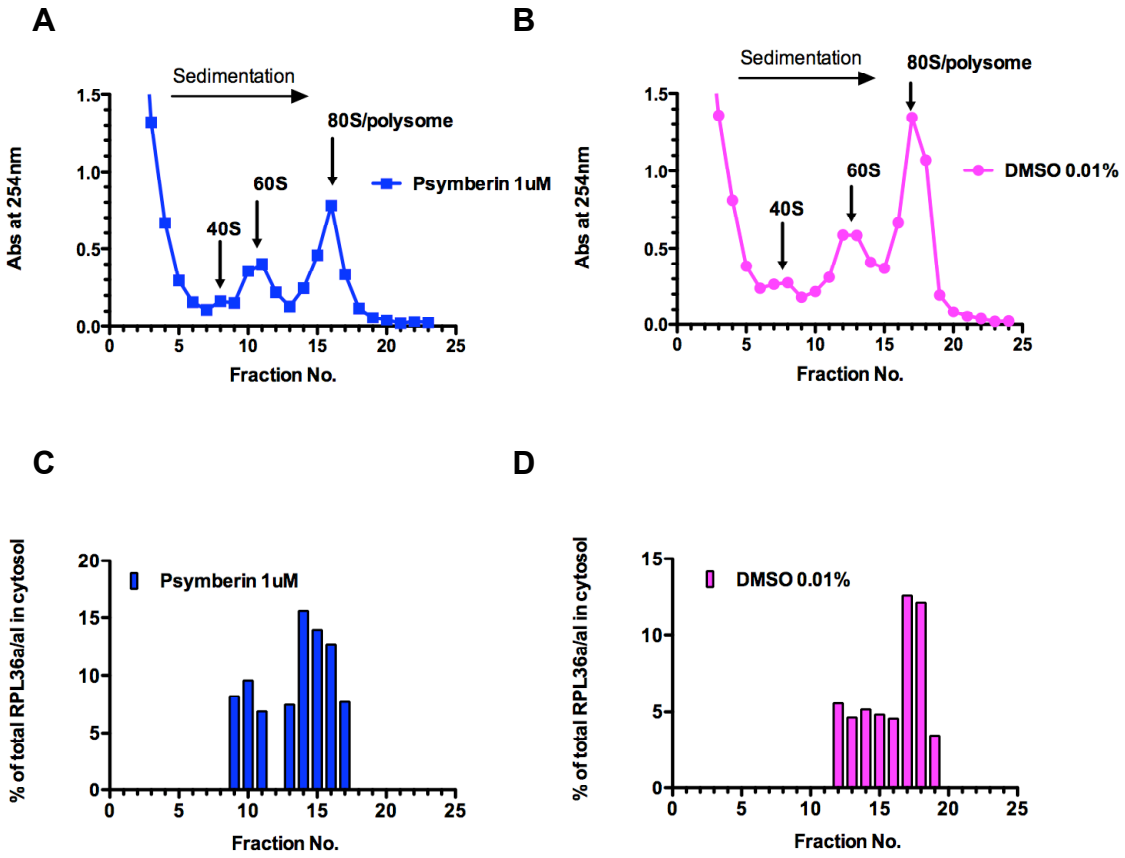

Figure 4.4 The profile of ribosome subunits in the cytosolic fraction of HeLa cells with and without psymberin treatment does not change. A and B, the cytosolic ribosome profile from HeLa cells treated with psymberin (A) or DMSO (B). C and D. the RPL36a content in each fraction was quantified by western blot.

4.3 The Effects of Psymberin in Cell Death Pathways Other Than Apoptosis

To search for causes of fast cell death induced by psymberin in addition to apoptosis and the inhibition of protein synthesis, other cell death pathways were studied in cells treated with psymberin. Mycalamide A was included for comparison to determine if any differences were related to the differences in side chain structure. First, induction of autophagy was examined. LC3 is a cytosolic protein that is converted to LC3-phosphatidylethanoalamine conjugate (LC3-II) when autophagy is induced under conditions of nutrient deprivation. The increase in LC3-II levels indicates induction of autophagy (95). However, there is endogenous LC3-II in some cell lines, including HeLa, under normal conditions (96). The amount of LC3-II was examined in HeLa cells treated with psymberin, mycalamide A or cycloheximide for different periods. Cells starved in PBS containing 2% DMEM were included as a positive control. The result is shown in Figure 4.5. The LC3 protein level decreased by time in cells treated with three protein synthesis inhibitors. The protein level of endogenous LC3-II in psymberin treated cells decreased significantly in the first hour and slowed down afterwards, whereas the starved cell (PBS treated) showed increased content of endogenous LC3-II, especially at the maximum at 2 hrs. Mycalamide A increased the levels of both LC3 and LC3-II in the first hour and cleared both of them at a slower rate compared to psymberin. Cycloheximide showed similar behavior to psymberin.

But the decay of endogenous LC3-II protein level in mycalamide A treated cells was slower at 4 hrs compared to psymberin. Interestingly, LC3-II level in psymberin-treated cells was lower than in cells treated with the other two translation inhibitors. These data suggested that psymberin did not induce autophagy, and there might be difference in mode of action between psymberin and mycalamide A in LC3 regulation and modification.

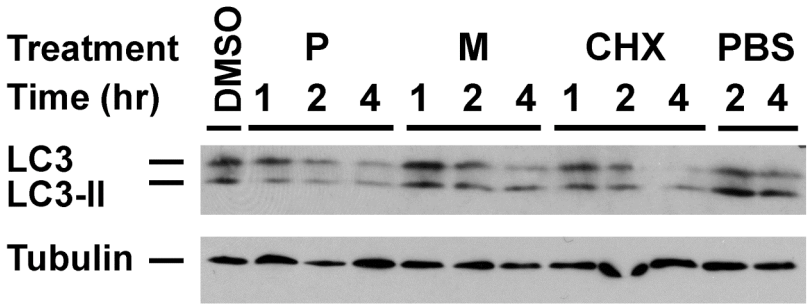

Figure 4.5 Psymberin does not induce autophagy. The LC3-II protein levels at indicated time from HeLa cells treated with psymberin (P), mycalamide A (M) and cycloheximide at >90% inhibition of protein synthesis were shown. PBS containing 2% DEME (PBS) was included as positive control.

Necrosis is another known cause of cell death. Recent advances in the study on necrosis suggest this process could be induced through a signaling network (97-99). I used an assay described in He et. al. (97) to investigate if psymberin

synergized with TNFα to induce necrosis. In this assay, the death signal induced in the apoptotic pathways by TNFα (T) and Smac (S) is blocked by Z-Vad-fmk (Z). However, even in the presence of Z-Vad-fmk the signal will go through the necrotic pathway to induce additional cell death, which is prevented by necrostatin (Figure 4.6). Mycalamide A was included for comparison. HT-29 cells were treated for 24 hrs with psymberin at a concentration that caused less than 10% inhibition of protein synthesis. When 10nM psymberin was substituted for Smac mimetic in the assay for TNFα-induced necrosis, necrostatin, a necrosis inhibitor, partially protected cells treated with the combination of psymberin (P), TNFα and Z-Vad-fmk, but not if mycalamide or cycloheximide replaced psymberin (Figure 4.6A). Because there was no significant necrotic cell death in P+T+Z treated cells, HT-29 cells were treated with drug at more than 90% inhibition of translation for 48 hrs, which is a standard condition in cell viability assays. Psymberin promoted TNFα-induced necrotic cell death in HT-29 cells which could be partially rescued by necrostatin. In the same conditions, mycalamide A could not promote TNFα-induced necrotic cell death (Figure 4.6B). But necrostatin partially rescues the cell death induced both by TNFα and mycalamide A (Figure 4.6B, M+T+Z and M+T+Z+N). Cycloheximide induced more cell death with TNFα, but there was no additional death in the presence of Z-Vad-fmk. Both psymberin and mycalamide A failed to induce necrotic cell death without the presence of TNFα (Figure 4.6B, P+Z and M+Z). These data

suggest that at >90% inhibition of translation, psymberin promoted TNFα-induced necrotic cell death that distinguished it from mycalamide A and cycloheximide.

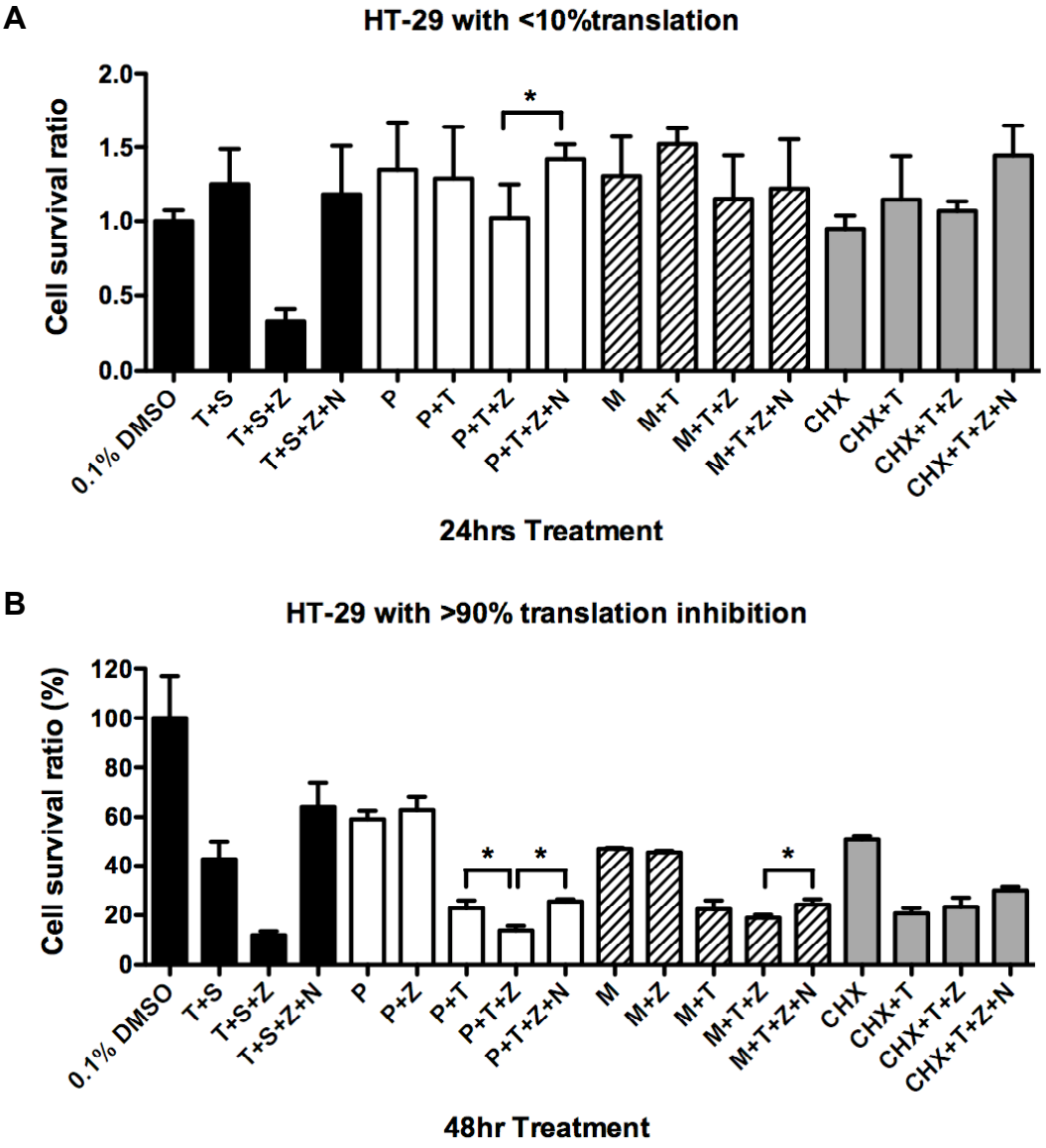

Figure 4.6 Psymberin promoted the TNFα-induced necrosis in HT-29 cells. The HT-29 cells were treated with A. <10% inhibition of translation for 24 hrs, and B. >90% inhibition of translation for 48 hrs. The concentrations of TNFα (T, 20ng/ml), Z-Vad-fmk (Z, 20mM), Smac mimetic (S, 100nM), and necrostatin (N, 10μM) were the same in two experiments. The concentrations of psymberin (P) were 10nM and 1μM; mycalamide A, 10nM and 1μM; cycloheximide 1μM and 100μM, in two experiments, respectively. * p<0.05.

4.4 Discussion

Surprisingly, the psymberin-resistant mutation in worms may only slightly reduce the binding of psymberin to the ribosome, because the change in K_d was only 50% and not significant at a 95% confidence level. The change of a proline to a leucine would be predicted to increase the flexibility of the polypeptide chain in the region of the mutation. A more flexible conformation in the binding pocket might allow the protein to undergo conformational changes necessary for translation with psymberin bound. One way to rationalize a possible explanation for the impact of the structural change in mutant RPL36a would be to study the alignment of a mammalian ribosome with an archaeal ribosome, where the binding of the pederin family member mycalamide has been visualized (28). Since there is no true mammalian ribosome crystal structure available, I can only use a computer-generated canine ribosome structure derived from electron density maps obtained by Cryo-EM. In the aligned structures of mammalian RPL36a and archaeal L44e, the distance of the two conserved lysines, which provide two possible hydrogen bonds between mycalamide A and L44e in the archaeal ribosome, are changed in the mammalian ribosome and may no longer contribute to binding (Figure 4.7). Even should the binding conformation of mycalamide A be similar in the two ribosomes, the terminal hydroxyl group of mycalamide A would form only one hydrogen bond with a carbonyl group on the backbone of

the loop that contains the psymberin-resistant change in RPL36a. On the other hand, the conformation of the 25S rRNA in mammalian ribosomes is different from that of the 23S rRNA in the archaeal ribosome (Figure 4.8). The orientations in space of the tRNAs at E-site in the two ribosomes are also different. Therefore, if mycalamide functions in the mammalian ribosome as it does in the archaeal ribosome, the binding conformation of mycalamide A may be rotated down so that the tetrahydropyran core and the ethylene dihydroxl side chain fill the space that would be occupied by the t-RNA CCA terminus. The hydroxyl groups on the amidyl side chain of mycalamide A may interact with the RNA nucleotides C3893 and U3894 in mammalian ribosomes, similar to interactions between mycalamide A and C2394 and C2395 in archaeal ribosomes. These potential interactions may stabilize the binding. As for the possible conformational change in the binding pocket in the presence of psymberin, there are several aromatic residues on the loop around the proline at the mutation site that could provide Van der Waals or π-π interactions with the dihydroisocoumarin side chain of psymberin. The most likely one is the Phe67 following the proline in this sequence (Figure 3.12). In addition, the nucleotide C92 of the 25S rRNA may also interact with the dihydroisocoumarin moiety. RPL36al was shown to interact with the CCA terminus of the tRNA at the P-site (100). These possible interactions may help psymberin to lock the conformation of the loop during the translocation of tRNA from P-site to E-site. The structural change from a rigid proline to a

relatively free leucine may interrupt these interactions resulting in lowering the energy gap for the conformational change of RPL36a in psymberin-bound mutant ribosomes during the tRNA translocation. This may also be a possible reason why the leucine mutation only contributes to psymberin-specific resistance, because the hydrogen bounds of mycalamide A may not be affected by the conformational change in the loop containing the mutation site.

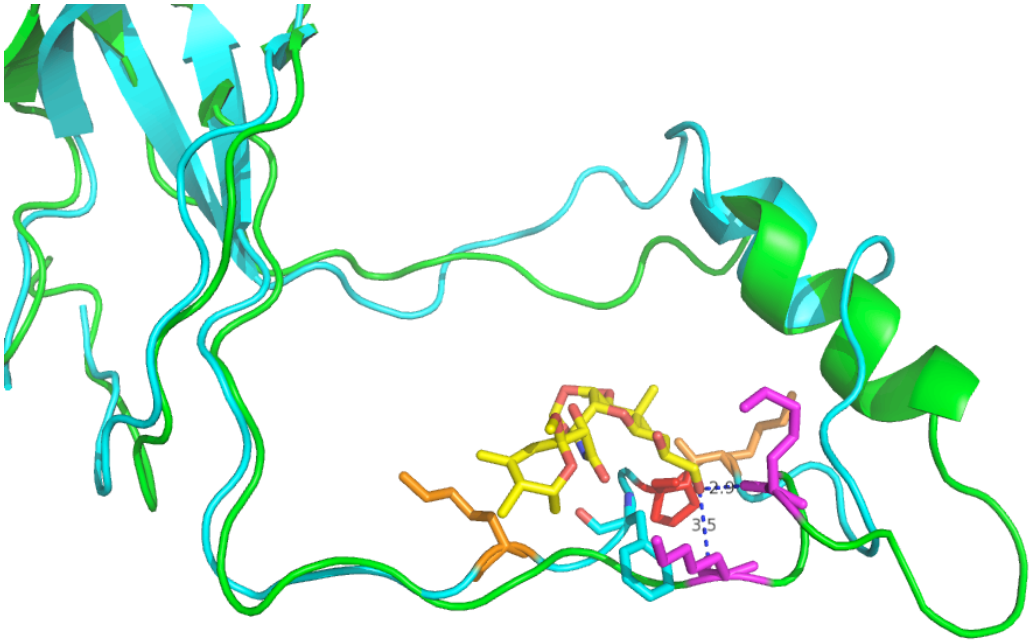

Figure 4.7 The aligned structures of RPL36a and L44e at the mycalamide A binding site. The mycalamide A (yellow) binding site in the ribosome close to L44e (green) is aligned with RPL36a (cyan). The proline in red is the mutation site, flanked by two conserved lysines (orange in RPL36a and pink in L44e). The number indicates the distance in Å between atoms. A. The alignment

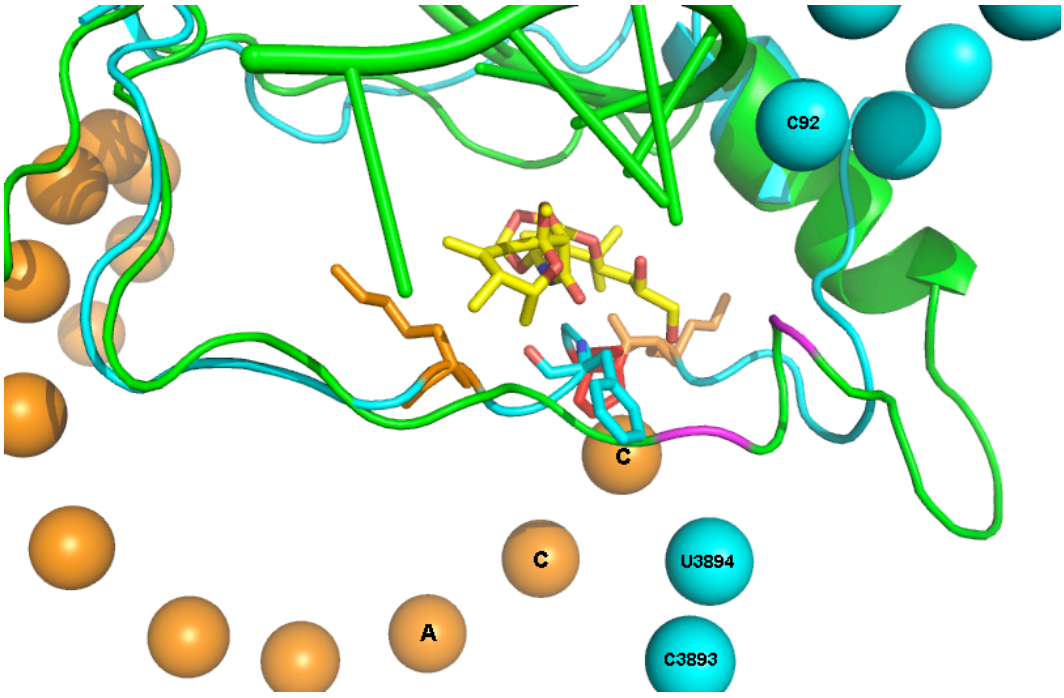

Figure 4.8 The binding conformation of psymberin and mycalamide A in eukaryotic ribosome may be different from that in archaeal ribosome. The aligned structures of RPL36a and L44e at the mycalamide A binding site. The mycalamide A (yellow) binding site in the ribosome close to L44e (green) is aligned with RPL36a (cyan). The proline in red is the mutation site, flanked by two conserved lysines (orange in RPL36a and pink in L44e). The cyan balls represent the 25S rRNA in mammalian ribosome, orange balls the CCA terminus of tRNA at E-site in mammalian ribosome. Residues on green helix are from 23S rRNA.

To search for the possible additional causes contributing to fast cell death induced by psymberin, I studied the effect of psymberin on ribosome assembly. Ribosome assembly is a complex process having multiple layers of regulation. Both the small and large subunits are synthesized in the nucleus before being exported to

the cytosol and assembled into a functional ribosome on a mRNA. The ribosome is disassembled after translation termination and recycled for the next event of translation (101). Therefore, the ribosome is catabolized as a unit with a long turnover time, about 75 hrs in rat liver cells. The synthesis of ribosomes occurs at about 1081 ribosome/min/cell in the same tissue (102). A recent study of mycalamide B suggested that mycalamide B is capable of changing the polysome profile and increasing 80S content obtained in a whole HEK293KT cell lysate (103). The effect of psymberin in ribosome assembly is different. Due to the lack of continuous flow-through spectrometer, I could only separate gradients into fractions making it is harder to obtain a polysome profile. However, I did not observe either an increase in 80S content, or change of the ribosome profile from cytosol when cells were treated with psymberin. Similar to the cytosolic faction, the ribosome profile in the nucleus was not changed, although both 40S and 60S content were decreased (Figure 4.4). These data suggested that psymberin does not affect the ribosome assembly process, but possibly the regulation of subunit synthesis. However, this effect of psymberin may not contribute to the fast killing property due to the long half-life of ribosomes.

Next, the effects of psymberin in other cell death pathways were examined. The difference in side chain structure also contributes to biological activities other than binding to the ribosome. Cycloheximide and puromycin inhibit the

autophagy in mouse liver and pancreatic cells through unknown mechanisms although it has been suggested that this might be due to decreased synthesis of proteins that regulates the autophagy response (104). However, my data suggested that there is no accumulation of LC3-II upon psymberin treatment. The change of endogenous LC3-II levels in HeLa cell differed between psymberin and mycalamide A treatments that should have inhibited protein synthesis equally. Mycalamide A appeared to induce LC3 and LC3-II after 1 hour and psymberin did not, suggesting that these compounds differ in more than inhibiting translation. As for the necrotic cell death, there is growing evidence of cross-talk between apoptosis and necrosis in the mechanism of cell death in several disease models, such as heart, diabetes, neurodegenerative diseases (98, 105, 106). Psymberin has been shown to induce apoptosis through ribotoxic stress (107). In our study, psymberin induced additional cell death in the presence of TNFα. Necrotic cell death was also observed when apoptosis was blocked in the presence of psymberin, TNFα and Z-Vad-fmk, suggesting that psymberin may function like Smac to induce an apoptotic signal, and that blocking this apoptotic signal triggers necrotic cell death. Our data suggested that psymberin acts differently from mycalamide A in TNFα–induced necrotic cell death. The dihydroisocoumarin side chain may play an important role to signal for both apoptotic and necrotic cell death.

Chapter Five

Conclusion and Future Directions

Psymberin is a unique compound in the pederin family not only because of its structure, but also its additional biological activities. There are several studies showing that a slight change in substitution or stereochemistry affects the toxicity of psymberin greatly (73, 77, 84). However, our thorough SAR study suggests that these alterations of the toxin are more likely due to changes in the transportation or degradation of the compound resulting indirectly in changes to the both toxicity and the inhibition of protein synthesis. The pederic acid moiety is important for the biological activities of other pederin family members (103), but our SAR suggests that the chiral hydroxyl groups are important, as well as the dihydroisocoumarin. Based on the SAR studies done by us and others (77), the double bond in the end of amidyl side chain is also important to toxicity. Structural integrity is also important. The ribosome binding experiment showed that lost of either side chain of psymberin dramatically reduced the binding affinity to ribosomes. On the other hand, our SAR study suggested that the toxicity and inhibition of protein synthesis could be uncoupled. This has been reported before in the case of shiga toxins (Stx1 and Stx2), which are ribosome inactivating proteins. Shiga toxins cleave an adenine from the highly conserved

α-sacrin ricin loop of the large rRNA. The cytotoxicity comes from the substructure in the C-terminus that is responsible for the transportation of toxin. Deletion of the C-terminus attenuated cytotoxicity but not inhibition of translation (108). From our SAR study, the substitution of dihydroisocoumarin with the pederin dihydroxyl ethylene moiety gave no more than a 3-fold change in inhibition of protein synthesis compared to psymberin, but more than a 1,000 fold change in cytotoxicity. Therefore, the dihydroisocoumarin side chain on psymberin is more important in inducing cytotoxicity.

To identify the molecular targets of psymberin, two separate forward genetic screens in *C. elegans* were performed. The only molecular target we identified was RPL41, the homolog of mammalian RPL36a/al. We had expected to find multiple targets of psymberin, yet in *C. elegans*, we repeatedly found a single point mutation. The failure to discover other mutations in two separate, large scale screens suggests strongly that the mutation we found in worms RPL41 is the only mutation that allows the ribosome to function in the presence of the drug.

We are the first group to provide evidence that RPL36a is the target of psymberin. The P65L point mutation confers resistance to psymberin in worms may cause slightly weaker binding of psymberin to the ribosome and this mutation is psymberin-specific. Based on a structural alignment analysis, the interaction of

the dihydroisocoumarin to RPL41/RPL36a(al) might be weakened because of the proline to leucine transition. The orientation of Phe67 may be different in the mutant ribosome reducing a potential π-π interaction to the dihydroisocoumarin. This kind of aromatic interaction contributes at least 2k/mol energy stabilization in biological systems (109). Losing this possible interaction may allow a the conformational change in RPL41 during tRNA translocation. On the other hand, this interaction would not be predicted for mycalamide A because the side chain of mycalamide A from C14 to C16 may be surrounded by a loop in RPL36a sequence that may not change conformation in mutant RPL36a. However, the conformation of the rRNA in eukaryotic ribosome may be different from the archaeal one. If so, the binding conformation of mycalamide A on the archaeal ribosome may only suggest the types of interactions that can stabilize binding, but not indicate the real conformation in the eukaryotic ribosome. The answers to these questions probably requires obtaining higher resolution structures of mammalian ribosomes with these inhibitors bound.

In searching for causes that induce fast cell death in addition to inhibition of translation, ribotoxic effects (107) and apoptosis (77), I obtained data suggesting that psymberin promotes TNFα-induced cell death, but not autophagy. However, psymberin may affect the regulation of chronically expressed LC3-II. In HeLa cell, the existence of endogenous LC3-II may indicate that autophagy is

constitutively turned on to eliminate waste from fast growth. With psymberin treatment, the LC3-II level dropped dramatically in one hour, faster than in cells treated with mycalamide and cycloheximide. Cycloheximide has been shown to reduce autophagy in rat liver and pancreatic cells (104, 110) by stopping the transportation of lysosomal enzymes to the lysosome, which should not affect the level of LC3-II. Our data suggested that there may be additional regulation of the synthesis or the degradation of LC3-II induced by psymberin. As for the TNFα-induced necrosis, psymberin could substitute for Smac to promote necrotic cell death but mycalamide A could not. Both mycalamide A (111) and psymberin could induce apoptosis. It is known that TNFα-induced stress also activates JNK, but through a different upstream pathway than does ribotoxic stress caused by UV and anisomycin (112). In our study, the ability to promote TNFα-induced necrosis resides in psymberin but not mycalamide A or cycloheximide. These data suggested that psymberin may activate JNK through additional signaling pathways different from the rest of the pederin family, and the apoptotic signal from psymberin could enhance the TNFα-induced necrosis. This promotion of TNFα-induced necrosis by psymberin suggests that dihydroisocoumarin may play a role in the induction of TNFα-induced necrosis. In conclusion, the dihydroisocoumarin provides unique properties to psymberin that contribute additional modes of actions and makes psymberin a potent toxin capable of inducing cell death through multiple pathways.

Several questions were raised during this study. Since the mutation in DA2312 is psymberin-specific, what is the exact difference in the binding conformation of psymberin between the wild-type and the mutant ribosome? One could prepare a psymberin-ribosome co-crystal to answer this question. This question is interesting, because the change in apparent affinity for ribosomes caused by the mutation is much less than the change in resistance to the toxin.

Ribotoxic stress is one of the causes of psymberin-induced cell death. Our SAR study suggests that inhibition of translation and toxicity could be uncoupled as shown by psympederin. It will be interesting to know if psympederin has attenuated activities on other pathways. To date, there is still a missing link in our understanding of the ribotoxic stress response in cells. JNK is only the mediator of signals. What is the messenger to deliver the stress signal from rRNA to the stress response protein? How is the stress signal delivered? And for the autophagy regulation, how does psymberin induce the fast clearance of endogenous LC3-II? Using psymberin and mycalamide A that differ in these responses as a molecular probes may provide answers to these questions.

This study provides a good base for further study in ribosome dynamics or biogenesis. In addition, in our preliminary study, a modification of the

dihydroisocoumarin side chain successfully increased the toxicity and translation inhibition by almost 1,000 fold compared to psymberin. Understanding the molecular mechanism behind this phenomenon could provide new details in our understanding of the molecular mechanism of protein translation.

Methods and Materials

Cell Lines and Reagents

All cell lines tested were purchased from American Type Culture Collection (Manassas, VA). SK-MEL-5 cells were grown in Dulbecco's modified Eagle's medium (DMEM; Hyclone) supplemented with 10% FBS (Atlanta Biological), 1mM sodium pyruvate, (GIBCO), 2mM glutamine (Invitrogen) and 0.1mM MEM non-essential amino acid (Invitrogen). HeLa and HT-29 cells were cultured in DMEM supplemented with 10% FBS, 1mM sodium pyruvate, and 10 mM HEPES. All culture media contained 1% of penicillin–streptomycin solution (Invitrogen).

Drugs and Antibodies

Paclitaxel (taxol), cycloheximide, NAC and Z-Vad-fmk are commercially available (Sigma-Aldrich). TNF-α and Smac mimetic are kind gifts from Xiaodong Wang (University of Texas Southwestern Medical Center/National Institute of Biological Science). Psymberin and analogs were synthesized by Jef De Brabander (University of Texas Southwestern Medical Center). Stock solutions were prepared in DMSO and stored at -80°C. Working dilutions were prepared fresh in M9 buffer or medium before experiments. Monocolonal anti-

RPL36a (Sigma-Aldrich), monocolonal anti-tublin (Sigma-Aldrich), and polycolonal anti-LC3 (Abcam) were obtained from commercial sources.

Protein Synthesis Inhibition Assay

To characterize the effect of drugs on protein synthesis, 40,000 cells were plated in each well of 12-well tissue culture plates. The next day, cells were incubated with various concentrations of compound in DMEM lacking cysteine and methionine for 20 min at 37°C, and then cells were radioactively labeled in the presence of compound by addition of 100mCi/ml TRAN ^{35}S-LABEL™ (MP Biomedicals) for 40 min at 37°C. After labeling, cells were chilled on ice, rinsed once with cold PBS and lysed in lysis buffer containing 1% Nonidet P-40; 50mM Tris; 0.1% SDS at pH 8.0 for 15 minutes on ice. The lysate was centrifuged at 20,800 x g for 10 minutes. 10 ml of the supernatant was spotted on Whatman filter paper. After drying, the filter paper was soaked in 10% tricholoroacetic acid (TCA) for 30 min, followed by washing briefly with 10% TCA twice, 1:1 EtOH: ether twice and ether twice. The radioactivity on each filter was counted with a LS-6500 scintillation counter (Beckman Coulter).

***in vitro* Translation Assay**

Rabbit Reticulocyte Lysate Translation System (Promega) was used to determine the effect of compounds on translation in a cell-free assay. All reagents are

provided in the kit, except compounds. The reactions were carried out in 0.2 ml RNase free tubes containing 9 µl of rabbit reticulocyte lysate, 0.25µl of amino acid mixture, 0.25µl of RNase inhibitor + RNasin, 0.5 µl luciferase control RNA, 1.5µl of water and 1µl of compound in various concentration. The translation reactions were incubated at 30°C for 90 minutes. The reaction mixtures were diluted to 50 µl with water containing 1mg/ml BSA for the standard luciferase assay. 2.5 µl of the diluted reaction mixture and 5 µl of luciferase assay reagent were mixed in a well containing 32.5µl of water containing 1mg/ml BSA in 96-well plate. The luminescence was measured by using a 96-well plate reader (Bio-Tek Instruments).

C. elegans culture and mating

The *C. elegans* were cultured according to modification of protocols from WormBook (113) as published by our lab (88). For the genetic mapping experiments, the worm strains used are the Hawaiian strain CB4856 and Bristol background mutant strains CB128 *dpy-10* (e128) II and CB91 *rol-1* (e91) II. For genetic mapping, hermaphrodites at the L4 stage were mated with a psymberin-resistant mutant males at a 1:2 ratio on NGM plates. The drug-resistant progeny were selected by growth in 5µM psymberin in liquid culture in 48-well plates.

Forward genetic screen for psymberin-resistant mutant

The protocol for the screen was modified from (88). Approximately 50,000 N2 late L4 worms were treated with 35mM of ethyl methansulfonate (Sigma-Aldrich) for 4hrs. One million L1 F2 progeny of the mutagenized parents were treated with 4.5 μM or 5μM of psymberin. The viable worms were tested in a second round of drug selection in 5μM of psymberin. Seven worms were selected individually from two independent screens.

SNP mapping of *rpl-41(ad2312sd) II*

The method was modified from the literature (88). In brief, to perform SNP mapping, male DA2312 were crossed with the Hawaiian strain to generate 106 psymberin-resistant F2 progeny. The linkage map was determined by amplifying the DNA segment around the SNP sites listed in Table V, followed by digestion with the indicated restriction enzyme. To narrow down the region containing the mutation, two visible markers, *dpy-10* and *rol-1*, were used to flank the drug-resistance mutation for modified three-point mapping (114). Psymberin-resistant double mutants were mated with Hawaiian strain worms and psymberin-resistant F2 progeny lacking the visible marker (recombinants) were selected for SNP analysis. Those progeny were examined at the SNP sites listed in Table V to determine the region linked to psymberin-resistant mutation (the region that was

never Hawaiian). The region between +3.1cM and +3.5cM on chromosome II was identified as linked to the psymberin-resistant mutation.

Table V. The SNP sites* examined in the genetic mapping.

Chromosome	Allele**	Location on chromosome (cM)	Restriction Enzyme
I	*pkP1057*	+1.01	NdeI
II	*pkP2101*	-15.90	DraI
II	*pkP2107*	+0.11	DraI
II	*pkP2109*	+1.38	EcoRI
II	*snp_C05C10[1]*	+1.77	MnII
II	*pkP2129*	+3.09	DdeI
II	*snp_C47G2[1]*	+3.35	DraI
II	*snp_B0334[1]*	+3.5	DpnI
II	*snp_F44E5[2]*	+4.04	MseI
II	*snp_ZK930[3]*	+4.11	HaeIII
II	*snp_Y17G7B[7]*	+5.9	DdeI
II	*snp_Y57A10A[2]*	+6.75	KpnI
II	*pkP2111*	+8.15	EcoRI
II	*snp_F15D4[6]*	+15.77	DraI
III	*pkP3096*	-4.13	EcoRI
IV	*haw65131*	+1.40	DraI
V	*pkP5097*	+0.55	DraI
X	*snp_F45E1[1]*	-0.77	EcoRI

*Data are from the online database at the following URL,
http://genome.wustl.edu/genome_data/c._elegans_single_nucleotide_polymorphism_data
**Data from www.wormbase.org

Sequencing of *rpl-41*

A 1.79kb fragment of genomic DNA from the DA2312 mutant, covering the sequence from base pairs 11096380 to 11098167 of chromosome II, was amplified and sequenced. We identify only a single point mutation in the C09H10.2 (*rpl-41*) gene. The following primers were used for amplification: forward, TTTATGCCATTGATGGGCAT and TCCGAGCTCGAAGTGTTTG; reverse, ACAAGGTTACCCAATACAAG and ACCAGAAGTTTTGAGTTC-TCC.

Microinjection to confirm phenotype

A 1787-bp PCR product spanning the *rpl-41* locus with 1019 bp of upstream sequence and 129 bp of downstream sequence was amplified from pCR2.1cosmid DNA. The PCR product was co-injected into N2 worms at a concentration of 20 ng/μl with *rol-6* (100ng/μl). 17 independent stable transgenic lines were isolated, and 16 of them were resistant to 2μM psymberin.

Drug toxicity experiments with worms

Worms were tested for sensitivity to toxins as described (88). The DMSO concentration in all experiments was kept below 1%.

Worm ribosome binding experiment

80S ribosomes from wild-type N2 and DA2312 worms were prepared as described (115). 0.4 unit/ml of RNaseOUT recombinant ribonuclease inhibitor (Invitrogen) and 1X protease inhibitor cocktail (Roche) were added to the ribosome preparation. The binding of psymberin to worm ribosomes was measured by a method modified from (26). In brief, 100nM ribosomes was incubated with various concentration of psymberin in a ribosome buffer (2.5mM $Mg(OAc)_2$, 100mM KOAc, 20mM HEPES at pH 7.6) containing 1mg/ml Heparin (Sigma-Aldrich) and 1X protease inhibitor cocktail (Roche) in a total volume of 110μl for 30min at 30°C. The reaction mixtures were ultracentrifuged at 400,000 × g at 4°C for 20 min. 100μl of supernatant was mixed with 100μl of methanol containing 0.2% formic acid. The insoluble salt was pelleted at 20,800 × g at 4°C for 5 min. 180μl of supernatant was transferred to a sample vial and subjected to LC-MS analysis to quantify the amount of free psymberin in the solution. The binding affinity was obtained by fitting the data with the equation for "one specific site – various sloop" using Prizm software (GraphPad).

Ribosomal assembly assay

A published method (116) was modified as follows. In brief, HeLa cells cultured in 150-mm tissue culture plates were rinsed with cold PBS twice and then

collected in a 15-ml conical-bottom tube on ice. The cells were pelleted by centrifuging 5 min at 500× g at 4°C. The cell pellet was resuspended in 2 ml ice-cold sterile LSB (10mM HEPES-NaOH, pH 7,5; 10mM NaCl; 2mM $MgCl_2$; 1mM EGTA) and incubated on ice for 10min. After incubation, the cells were pelleted and resuspened in 2 ml LSB+ (LSB plus 5μl/ml of protease inhibitor cocktail (Roche)). 66 μl of 10% NP-40 (CaliboChem) and 44 μl of 10% sodium deoxycholate (Sigma-Aldrich) were added sequentially and the sample was vortexed vigorously. The nuclei were sedimented at 1000× g, 4°C for 5 min. The cytosolic supernatant was transferred to the top of a 10-60% sucrose gradient. The gradient was ultracentrifuged for 3 hr at 160,000 × g at 4°C. 500-μl fractions of the gradient were collected at 4°C with an Auto Densi-Flow II C fractionator (Buchler Instrument). The A_{254} of each fraction was monitored by using a NanoDrop 1000 UV/Vis spectrophotometer (Thermo Scientific). The nuclear extract was prepared as described (116), followed by the same sucrose gradient sedimentation above to obtain the A_{260} of each fraction.

Western blot

Cells were cultured with drugs in a 6-well plate. Cells in each well were lysed with 150 μl of 10mM Tris, pH 6.8 containing 20% glycerol, 0.6% SDS, 10% 2-mercaptoethanol and 0.1% bromophenol blue, and boiled for 5 minutes before

loading on a 15% acrylamide SDS-PAGE gel. After samples were separated, the proteins were transferred from the gel by electrophoresis to a nitrocellulose membrane (BIO-RAD) and blocked with 5% non-fat milk (LabScientific) in PBS (MediaTech Inc.) containing 0.1% TWEEN-20 (Sigma-Aldrich) for 45 min. The membrane was incubated with primary antibody under conditions recommended by the vendor, followed by three washes with 1X PBS containing 0.1% TWEEN-20. The membrane was then incubated with the appropriate HRP-conjugated secondary antibody for 1 hr at room temperature. After washing three times with PBS containing 0.1% TWEEN-20, the protein bands that had bound antibody were detected by a chemoluminescence reaction and visualized on autoradiography film.

Assay for TNF-α induced necrotic cell death

The method described previously in He et. al was followed (97). Cells were cultured in a 96-well plate and treated with drugs at the indicated concentrations and times. Cell viability was determined by CellTiter-Glow® assay (Promega).

References

1. Newman DJ & Cragg GM (2007) Natural products as sources of new drugs over the last 25 years. (Translated from eng) *Journal of natural products* 70(3):461-477 (in eng).
2. Solecki RS (1975) Shanidar IV, a Neanderthal Flower Burial in Northern Iraq. *Science* 190(4217):880-881.
3. Galeano E, Rojas JJ, & Martinez A (2011) Pharmacological developments obtained from marine natural products and current pipeline perspective. (Translated from eng) *Natural product communications* 6(2):287-300 (in eng).
4. Waters AL, Hill RT, Place AR, & Hamann MT (2010) The expanding role of marine microbes in pharmaceutical development. (Translated from eng) *Current opinion in biotechnology* 21(6):780-786 (in eng).
5. Piel J, *et al*. (2005) Exploring the chemistry of uncultivated bacterial symbionts: antitumor polyketides of the pederin family. (Translated from eng) *Journal of natural products* 68(3):472-479 (in eng).
6. Pavan M & Bo G (1953) *Physiologia comp. Oecol*. 3:307.
7. Cardani C, Ghiringh.D, Quilico A, & Selva A (1967) Structure of Pederone a Novel Substance from Paederus (Coleoptera Staphylinidae). (Translated from English) *Tetrahedron Lett* (41):4023-& (in English).
8. Frank JH & Kanamitsu K (1987) Paederus, sensu lato (Coleoptera: Staphylinidae): natural history and medical importance. (Translated from eng) *Journal of medical entomology* 24(2):155-191 (in eng).
9. Perry NB, Blunt JW, Munro MHG, & Pannell LK (1988) Mycalamide A, an antiviral compound from a New Zealand sponge of the genus Mycale. *Journal of the American Chemical Society* 110(14):4850-4851.
10. Perry NB, Blunt JW, Munro MHG, & Thompson AM (1990) Antiviral and Antitumor Agents from a New-Zealand Sponge, Mycale Sp .2. Structures and Solution Conformations of Mycalamide-a and Mycalamide-B. (Translated from English) *J Org Chem* 55(1):223-227 (in English).
11. Simpson JS, Garson MJ, Blunt JW, Munro MH, & Hooper JN (2000) Mycalamides C and D, cytotoxic compounds from the marine sponge Stylinos n. species. (Translated from eng) *Journal of natural products* 63(5):704-706 (in eng).

12. West LM, Northcote PT, Hood KA, Miller JH, & Page MJ (2000) Mycalamide D, a new cytotoxic amide from the New Zealand marine sponge Mycale species. (Translated from eng) *Journal of natural products* 63(5):707-709 (in eng).
13. Sakemi S, Ichiba T, Kohmoto S, Saucy G, & Higa T (1988) Isolation and Structure Elucidation of Onnamide-a, a New Bioactive Metabolite of a Marine Sponge, Theonella Sp. (Translated from English) *Journal of the American Chemical Society* 110(14):4851-4853 (in English).
14. Matsunaga S, Fusetani N, & Nakao Y (1992) 8 New Cytotoxic Metabolites Closely Related to Onnamide-a from 2 Marine Sponges of the Genus Theonella. (Translated from English) *Tetrahedron* 48(39):8369-8376 (in English).
15. Kobayashi J, Itagaki F, Shigemori H, & Sasaki T (1993) 3 New Onnamide Congeners from the Okinawan Marine Sponge Theonella Sp. (Translated from English) *Journal of natural products* 56(6):976-981 (in English).
16. Vuong D, *et al*. (2001) Onnamide F: a new nematocide from a southern Australian marine sponge, Trachycladus laevispirulifer. (Translated from eng) *Journal of natural products* 64(5):640-642 (in eng).
17. Fusetani N, Sugawara T, & Matsunaga S (1992) Bioactive Marine Metabolites Series .41. Theopederins-a-E, Potent Antitumor Metabolites from a Marine Sponge, Theonella Sp. (Translated from English) *J Org Chem* 57(14):3828-3832 (in English).
18. Tsukamoto S, Matsunaga S, Fusetani N, & Toh-E A (1999) Theopederins F-J: Five new antifungal and cytotoxic metabolites from the marine sponge, Theonella swinhoei. (Translated from English) *Tetrahedron* 55(48):13697-13702 (in English).
19. Paul GK, Gunasekera SP, Longley RE, & Pomponi SA (2002) Theopederins K and L. Highly potent cytotoxic metabolites from a marine sponge Discodermia species. (Translated from eng) *Journal of natural products* 65(1):59-61 (in eng).
20. Cichewicz RH, Valeriote FA, & Crews P (2004) Psymberin, a potent sponge-derived cytotoxin from Psammocinia distantly related to the pederin family. (Translated from eng) *Organic letters* 6(12):1951-1954 (in eng).
21. Pettit GR, *et al*. (2004) Antineoplastic agents. 520. Isolation and structure of irciniastatins A and B from the Indo-Pacific marine sponge Ircinia ramosa. (Translated from eng) *J Med Chem* 47(5):1149-1152 (in eng).
22. Piel J (2002) A polyketide synthase-peptide synthetase gene cluster from an uncultured bacterial symbiont of Paederus beetles. (Translated from eng) *Proc Natl Acad Sci U S A* 99(22):14002-14007 (in eng).

23. Patani GA & LaVoie EJ (1996) Bioisosterism: A Rational Approach in Drug Design. (Translated from Eng) *Chem Rev* 96(8):3147-3176 (in Eng).
24. Brega A, Falaschi A, De Carli L, & Pavan M (1968) Studies on the mechanism of action of pederine. (Translated from eng) *The Journal of cell biology* 36(3):485-496 (in eng).
25. Soldati M, Fioretti A, & Ghione M (1966) Cytotoxicity of pederin and some of its derivatives on cultured mammalian cells. (Translated from eng) *Experientia* 22(3):176-178 (in eng).
26. Nishimura S*, et al*. (2005) 13-Deoxytedanolide, a marine sponge-derived antitumor macrolide, binds to the 60S large ribosomal subunit. (Translated from eng) *Bioorganic & medicinal chemistry* 13(2):449-454 (in eng).
27. Burres NS & Clement JJ (1989) Antitumor activity and mechanism of action of the novel marine natural products mycalamide-A and -B and onnamide. (Translated from eng) *Cancer research* 49(11):2935-2940 (in eng).
28. Gurel G, Blaha G, Steitz TA, & Moore PB (2009) Structures of triacetyloleandomycin and mycalamide A bind to the large ribosomal subunit of Haloarcula marismortui. (Translated from eng) *Antimicrob Agents Chemother* 53(12):5010-5014 (in eng).
29. Kongsaeree P, Prabpai S, Sriubolmas N, Vongvein C, & Wiyakrutta S (2003) Antimalarial dihydroisocoumarins produced by Geotrichum sp., an endophytic fungus of Crassocephalum crepidioides. (Translated from eng) *Journal of natural products* 66(5):709-711 (in eng).
30. Kamisuki S*, et al*. (2007) Nodulisporol and Nodulisporone, novel specific inhibitors of human DNA polymerase lambda from a fungus, Nodulisporium sp. (Translated from eng) *Bioorganic & medicinal chemistry* 15(9):3109-3114 (in eng).
31. Guimaraes KG, de Souza Filho JD, Dos Mares-Guia TR, & Braga FC (2008) Dihydroisocoumarin from Xyris pterygoblephara active against dermatophyte fungi. (Translated from eng) *Phytochemistry* 69(2):439-444 (in eng).
32. Al-Anati L & Petzinger E (2006) Immunotoxic activity of ochratoxin A. (Translated from eng) *Journal of veterinary pharmacology and therapeutics* 29(2):79-90 (in eng).
33. Pfohl-Leszkowicz A & Manderville RA (2007) Ochratoxin A: An overview on toxicity and carcinogenicity in animals and humans. (Translated from eng) *Mol Nutr Food Res* 51(1):61-99 (in eng).
34. Schilter B*, et al*. (2005) Ochratoxin A: potential epigenetic mechanisms of toxicity and carcinogenicity. (Translated from eng) *Food Addit Contam* 22 Suppl 1:88-93 (in eng).

35. Benesic A, Mildenberger S, & Gekle M (2000) Nephritogenic ochratoxin A interferes with hormonal signalling in immortalized human kidney epithelial cells. (Translated from eng) *Pflugers Arch* 439(3):278-287 (in eng).
36. Endringer DC, Guimaraes KG, Kondratyuk TP, Pezzuto JM, & Braga FC (2008) Selective inhibition of aromatase by a dihydroisocoumarin from Xyris pterygoblephara. (Translated from eng) *Journal of natural products* 71(6):1082-1084 (in eng).
37. Iordanov MS, *et al*. (1997) Ribotoxic stress response: activation of the stress-activated protein kinase JNK1 by inhibitors of the peptidyl transferase reaction and by sequence-specific RNA damage to the alpha-sarcin/ricin loop in the 28S rRNA. *Mol. Cell. Biol.* 17(6):3373-3381.
38. Lee KH, *et al*. (2005) Inhibition of protein synthesis and activation of stress-activated protein kinases by onnamide A and theopederin B, antitumor marine natural products. (Translated from eng) *Cancer Sci* 96(6):357-364 (in eng).
39. Iordanov MS, *et al*. (1998) Ultraviolet radiation triggers the ribotoxic stress response in mammalian cells. (Translated from eng) *J Biol Chem* 273(25):15794-15803 (in eng).
40. Iordanov MS & Magun BE (1999) Different mechanisms of c-Jun NH(2)-terminal kinase-1 (JNK1) activation by ultraviolet-B radiation and by oxidative stressors. (Translated from eng) *J Biol Chem* 274(36):25801-25806 (in eng).
41. Davis RJ (2000) Signal transduction by the JNK group of MAP kinases. (Translated from eng) *Cell* 103(2):239-252 (in eng).
42. Ouyang DY, Wang YY, & Zheng YT (2005) Activation of c-Jun N-terminal kinases by ribotoxic stresses. (Translated from eng) *Cell Mol Immunol* 2(6):419-425 (in eng).
43. Zhang Q, *et al*. (2005) Molecular mechanism(s) of burn-induced insulin resistance in murine skeletal muscle: role of IRS phosphorylation. (Translated from eng) *Life sciences* 77(24):3068-3077 (in eng).
44. Fan M, Du L, Stone AA, Gilbert KM, & Chambers TC (2000) Modulation of mitogen-activated protein kinases and phosphorylation of Bcl-2 by vinblastine represent persistent forms of normal fluctuations at G2-M1. (Translated from eng) *Cancer research* 60(22):6403-6407 (in eng).
45. Polverino AJ & Patterson SD (1997) Selective activation of caspases during apoptotic induction in HL-60 cells. Effects Of a tetrapeptide inhibitor. (Translated from eng) *J Biol Chem* 272(11):7013-7021 (in eng).
46. Xia S, Li Y, Rosen EM, & Laterra J (2007) Ribotoxic stress sensitizes glioblastoma cells to death receptor induced apoptosis: requirements for c-

Jun NH2-terminal kinase and Bim. (Translated from eng) *Mol Cancer Res* 5(8):783-792 (in eng).

47. Sah NK, *et al*. (2003) Translation inhibitors sensitize prostate cancer cells to apoptosis induced by tumor necrosis factor-related apoptosis-inducing ligand (TRAIL) by activating c-Jun N-terminal kinase. (Translated from eng) *J Biol Chem* 278(23):20593-20602 (in eng).
48. Chambers JW & Lograsso PV (2011) Mitochondrial c-Jun N-terminal Kinase (JNK) Signaling Initiates Physiological Changes Resulting in Amplification of Reactive Oxygen Species Generation. (Translated from eng) *J Biol Chem* 286(18):16052-16062 (in eng).
49. Cai SX, Drewe J, & Kasibhatla S (2006) A chemical genetics approach for the discovery of apoptosis inducers: from phenotypic cell based HTS assay and structure-activity relationship studies, to identification of potential anticancer agents and molecular targets. (Translated from eng) *Curr Med Chem* 13(22):2627-2644 (in eng).
50. Lang M & Beck-Sickinger AG (2006) Structure-activity relationship studies: methods and ligand design for G-protein coupled peptide receptors. (Translated from eng) *Curr Protein Pept Sci* 7(4):335-353 (in eng).
51. Jorgensen WL (2009) Efficient drug lead discovery and optimization. (Translated from eng) *Acc Chem Res* 42(6):724-733 (in eng).
52. Pierre F, *et al*. (2011) Discovery and SAR of 5-(3-chlorophenylamino)benzo[c][2,6]naphthyridine-8-carboxylic acid (CX-4945), the first clinical stage inhibitor of protein kinase CK2 for the treatment of cancer. (Translated from eng) *J Med Chem* 54(2):635-654 (in eng).
53. Hubbard BK & Walsh CT (2003) Vancomycin assembly: nature's way. (Translated from eng) *Angew Chem Int Ed Engl* 42(7):730-765 (in eng).
54. Crowley BM & Boger DL (2006) Total synthesis and evaluation of [Psi[CH2NH]Tpg4]vancomycin aglycon: reengineering vancomycin for dual D-Ala-D-Ala and D-Ala-D-Lac binding. (Translated from eng) *J Am Chem Soc* 128(9):2885-2892 (in eng).
55. Crane CM & Boger DL (2009) Synthesis and evaluation of vancomycin aglycon analogues that bear modifications in the N-terminal D-leucyl amino acid. (Translated from eng) *J Med Chem* 52(5):1471-1476 (in eng).
56. Istvan ES & Deisenhofer J (2001) Structural mechanism for statin inhibition of HMG-CoA reductase. (Translated from eng) *Science* 292(5519):1160-1164 (in eng).
57. Endo A (1992) The discovery and development of HMG-CoA reductase inhibitors. (Translated from eng) *J Lipid Res* 33(11):1569-1582 (in eng).

58. White CM (2002) A review of the pharmacologic and pharmacokinetic aspects of rosuvastatin. (Translated from eng) *J Clin Pharmacol* 42(9):963-970 (in eng).
59. Kawasumi M & Nghiem P (2007) Chemical genetics: elucidating biological systems with small-molecule compounds. (Translated from eng) *The Journal of investigative dermatology* 127(7):1577-1584 (in eng).
60. Carroll PM, Dougherty B, Ross-Macdonald P, Browman K, & FitzGerald K (2003) Model systems in drug discovery: chemical genetics meets genomics. (Translated from eng) *Pharmacology & therapeutics* 99(2):183-220 (in eng).
61. Ho CH, *et al*. (2011) Combining functional genomics and chemical biology to identify targets of bioactive compounds. (Translated from eng) *Current opinion in chemical biology* 15(1):66-78 (in eng).
62. Kaletta T & Hengartner MO (2006) Finding function in novel targets: C. elegans as a model organism. (Translated from eng) *Nat Rev Drug Discov* 5(5):387-398 (in eng).
63. Tickoo S & Russell S (2002) Drosophila melanogaster as a model system for drug discovery and pathway screening. (Translated from eng) *Current opinion in pharmacology* 2(5):555-560 (in eng).
64. Brittijn SA, *et al*. (2009) Zebrafish development and regeneration: new tools for biomedical research. (Translated from eng) *The International journal of developmental biology* 53(5-6):835-850 (in eng).
65. Kile BT & Hilton DJ (2005) The art and design of genetic screens: mouse. (Translated from eng) *Nature reviews* 6(7):557-567 (in eng).
66. Consortium TCeS (1998) Genome sequence of the nematode C. elegans: a platform for investigating biology. (Translated from eng) *Science* 282(5396):2012-2018 (in eng).
67. Wood WB (1988) *The Nematode Caenorhabditis elegans* (Cold Spring Harbor Laboratory, Cold Spring Harbor, N.Y.) pp xiii, 667 p.
68. Riddle DL (1997) *C. elegans II* (Cold Spring Harbor Laboratory Press, Plainview, N.Y.) pp xvii, 1222 p.
69. Kipreos ET (2005) C. elegans cell cycles: invariance and stem cell divisions. (Translated from eng) *Nat Rev Mol Cell Biol* 6(10):766-776 (in eng).
70. Sonnhammer EL & Durbin R (1997) Analysis of protein domain families in Caenorhabditis elegans. (Translated from eng) *Genomics* 46(2):200-216 (in eng).
71. Lai CH, Chou CY, Ch'ang LY, Liu CS, & Lin W (2000) Identification of novel human genes evolutionarily conserved in Caenorhabditis elegans by comparative proteomics. (Translated from eng) *Genome Res* 10(5):703-713 (in eng).

72. O'Brien KP, Westerlund I, & Sonnhammer EL (2004) OrthoDisease: a database of human disease orthologs. (Translated from eng) *Hum Mutat* 24(2):112-119 (in eng).
73. Jiang X, Williams N, & De Brabander JK (2007) Synthesis of psymberin analogues: probing a functional correlation with the pederin/mycalamide family of natural products. (Translated from eng) *Organic letters* 9(2):227-230 (in eng).
74. Baliga BS, Pronczuk AW, & Munro HN (1969) Mechanism of cycloheximide inhibition of protein synthesis in a cell-free system prepared from rat liver. (Translated from eng) *J Biol Chem* 244(16):4480-4489 (in eng).
75. Tang D, Lahti JM, Grenet J, & Kidd VJ (1999) Cycloheximide-induced T-cell death is mediated by a Fas-associated death domain-dependent mechanism. (Translated from eng) *J Biol Chem* 274(11):7245-7252 (in eng).
76. Ito K, *et al*. (2006) Molecular mechanism investigation of cycloheximide-induced hepatocyte apoptosis in rat livers by morphological and microarray analysis. (Translated from eng) *Toxicology* 219(1-3):175-186 (in eng).
77. Huang X, *et al*. (2009) The discovery of potent antitumor agent C11-deoxypsymberin/irciniastatin A: total synthesis and biology of advanced psymberin analogs. (Translated from eng) *Organic letters* 11(4):867-870 (in eng).
78. Luo KQ, Yu VC, Pu Y, & Chang DC (2003) Measuring dynamics of caspase-8 activation in a single living HeLa cell during TNFalpha-induced apoptosis. (Translated from eng) *Biochem Biophys Res Commun* 304(2):217-222 (in eng).
79. Qu X & Qing L (2004) Abrin induces HeLa cell apoptosis by cytochrome c release and caspase activation. (Translated from eng) *J Biochem Mol Biol* 37(4):445-453 (in eng).
80. Hwang S, *et al*. (2011) Time-lapse, single cell based confocal imaging analysis of caspase activation and phosphatidylserine flipping during cellular apoptosis. (Translated from eng) *Biotech Histochem* 86(3):181-187 (in eng).
81. Ito T, Ando H, & Handa H (2011) Teratogenic effects of thalidomide: molecular mechanisms. (Translated from eng) *Cell Mol Life Sci* 68(9):1569-1579 (in eng).
82. Melchert M & List A (2007) The thalidomide saga. (Translated from eng) *Int J Biochem Cell Biol* 39(7-8):1489-1499 (in eng).

83. Ito T, *et al*. (2010) Identification of a primary target of thalidomide teratogenicity. (Translated from eng) *Science* 327(5971):1345-1350 (in eng).
84. Watanabe T, *et al*. (2010) Syntheses and biological evaluation of irciniastatin A and the C1-C2 alkyne analogue. (Translated from eng) *Organic letters* 12(5):1040-1043 (in eng).
85. Lehmler HJ, *et al*. (2010) Chiral polychlorinated biphenyl transport, metabolism, and distribution: a review. (Translated from eng) *Environ Sci Technol* 44(8):2757-2766 (in eng).
86. Sheps JA, Ralph S, Zhao Z, Baillie DL, & Ling V (2004) The ABC transporter gene family of Caenorhabditis elegans has implications for the evolutionary dynamics of multidrug resistance in eukaryotes. (Translated from eng) *Genome Biol* 5(3):R15 (in eng).
87. Broeks A, Gerrard B, Allikmets R, Dean M, & Plasterk RH (1996) Homologues of the human multidrug resistance genes MRP and MDR contribute to heavy metal resistance in the soil nematode Caenorhabditis elegans. (Translated from eng) *EMBO J* 15(22):6132-6143 (in eng).
88. Zubovych I, Doundoulakis T, Harran PG, & Roth MG (2006) A missense mutation in Caenorhabditis elegans prohibitin 2 confers an atypical multidrug resistance. (Translated from eng) *Proc Natl Acad Sci U S A* 103(42):15523-15528 (in eng).
89. Seidel HS, Rockman MV, & Kruglyak L (2008) Widespread genetic incompatibility in C. elegans maintained by balancing selection. (Translated from eng) *Science* 319(5863):589-594 (in eng).
90. Rockman MV & Kruglyak L (2009) Recombinational landscape and population genomics of Caenorhabditis elegans. (Translated from eng) *PLoS Genet* 5(3):e1000419 (in eng).
91. Greene EA, *et al*. (2003) Spectrum of chemically induced mutations from a large-scale reverse-genetic screen in Arabidopsis. (Translated from eng) *Genetics* 164(2):731-740 (in eng).
92. Zhou CC, Swaney SM, Shinabarger DL, & Stockman BJ (2002) 1H nuclear magnetic resonance study of oxazolidinone binding to bacterial ribosomes. (Translated from eng) *Antimicrob Agents Chemother* 46(3):625-629 (in eng).
93. Borovinskaya MA, *et al*. (2007) Structural basis for aminoglycoside inhibition of bacterial ribosome recycling. (Translated from eng) *Nat Struct Mol Biol* 14(8):727-732 (in eng).
94. Mehta R & Champney WS (2002) 30S ribosomal subunit assembly is a target for inhibition by aminoglycosides in Escherichia coli. (Translated from eng) *Antimicrob Agents Chemother* 46(5):1546-1549 (in eng).

95. Tanida I, Ueno T, & Kominami E (2008) LC3 and Autophagy. (Translated from eng) *Methods Mol Biol* 445:77-88 (in eng).
96. Tanida I, Minematsu-Ikeguchi N, Ueno T, & Kominami E (2005) Lysosomal turnover, but not a cellular level, of endogenous LC3 is a marker for autophagy. (Translated from eng) *Autophagy* 1(2):84-91 (in eng).
97. He S, *et al*. (2009) Receptor interacting protein kinase-3 determines cellular necrotic response to TNF-alpha. (Translated from eng) *Cell* 137(6):1100-1111 (in eng).
98. Kung G, Konstantinidis K, & Kitsis RN (2011) Programmed necrosis, not apoptosis, in the heart. (Translated from eng) *Circ Res* 108(8):1017-1036 (in eng).
99. Cho YS, *et al*. (2009) Phosphorylation-driven assembly of the RIP1-RIP3 complex regulates programmed necrosis and virus-induced inflammation. (Translated from eng) *Cell* 137(6):1112-1123 (in eng).
100. Baouz S, *et al*. (2009) The human large subunit ribosomal protein L36A-like contacts the CCA end of P-site bound tRNA. (Translated from eng) *Biochimie* 91(11-12):1420-1425 (in eng).
101. Fromont-Racine M, Senger B, Saveanu C, & Fasiolo F (2003) Ribosome assembly in eukaryotes. (Translated from eng) *Gene* 313:17-42 (in eng).
102. Nikolov EN, Dineva BB, Dabeva MD, & Nikolov TK (1987) Turnover of ribosomal proteins in regenerating rat liver after partial hepatectomy. (Translated from eng) *Int J Biochem* 19(2):159-163 (in eng).
103. Dang Y, *et al*. (2011) Inhibition of eukaryotic translation elongation by the antitumor natural product Mycalamide B. (Translated from Eng) *RNA* (in Eng).
104. Oliva O, Laszlo L, Palfia Z, & Rez G (1991) Translational inhibitors cycloheximide, emetine, and puromycin inhibit cellular autophagy in mouse liver parenchymal and pancreatic acinar cells in vivo. (Translated from eng) *Acta Morphol Hung* 39(2):79-85 (in eng).
105. Dorn GW, 2nd (2010) Mechanisms of non-apoptotic programmed cell death in diabetes and heart failure. (Translated from eng) *Cell Cycle* 9(17):3442-3448 (in eng).
106. Zhivotovsky B & Orrenius S (2010) Cell death mechanisms: cross-talk and role in disease. (Translated from eng) *Exp Cell Res* 316(8):1374-1383 (in eng).
107. Chinen T, *et al*. (2010) Irciniastatin A induces JNK activation that is involved in caspase-8-dependent apoptosis via the mitochondrial pathway. (Translated from eng) *Toxicology letters* 199(3):341-346 (in eng).

108. Di R, *et al*. (2011) Identification of amino acids critical for the cytotoxicity of Shiga toxin 1 and 2 in Saccharomyces cerevisiae. (Translated from eng) *Toxicon* 57(4):525-539 (in eng).
109. Boehr DD, Farley AR, Wright GD, & Cox JR (2002) Analysis of the pi-pi stacking interactions between the aminoglycoside antibiotic kinase APH(3')-IIIa and its nucleotide ligands. (Translated from eng) *Chem Biol* 9(11):1209-1217 (in eng).
110. Lawrence BP & Brown WJ (1993) Inhibition of protein synthesis separates autophagic sequestration from the delivery of lysosomal enzymes. (Translated from eng) *J Cell Sci* 105 (Pt 2):473-480 (in eng).
111. Hood KA, West LM, Northcote PT, Berridge MV, & Miller JH (2001) Induction of apoptosis by the marine sponge (Mycale) metabolites, mycalamide A and pateamine. (Translated from eng) *Apoptosis* 6(3):207-219 (in eng).
112. Wang X, *et al*. (2005) Complete inhibition of anisomycin and UV radiation but not cytokine induced JNK and p38 activation by an aryl-substituted dihydropyrrolopyrazole quinoline and mixed lineage kinase 7 small interfering RNA. (Translated from eng) *J Biol Chem* 280(19):19298-19305 (in eng).
113. Stiernagle T (Maintenance of C. elegans. in *WormBook*, ed Community TCeR (WormBook).
114. Fay D (Genetic mapping and manipulation: Chapter 5-SNPs: Three-point mapping. in *WormBook*, ed Community TCeR (WormBook).
115. Algire MA, *et al*. (2002) Development and characterization of a reconstituted yeast translation initiation system. (Translated from eng) *RNA* 8(3):382-397 (in eng).
116. Pestov DG, Lapik YR, & Lau LF (2008) Assays for ribosomal RNA processing and ribosome assembly. (Translated from eng) *Curr Protoc Cell Biol* Chapter 22:Unit 22 11 (in eng).